

# Transient rebellions in the Kuramoto oscillator: Morse-Smale structural stability and connection graphs of finite 2-shift type

*Dedicated to Professor Yoshiki Kuramoto  
in celebration of the 50th anniversary  
of the classical Kuramoto oscillator*

Jia-Yuan Dai\*, Bernold Fiedler\*\*, Alejandro López-Nieto\*\*\*

version of December 3, 2025

\*

Department of Mathematics  
National Tsing Hua University  
No. 101, Sec. 2, Kuang-Fu Road  
Hsinchu, Taiwan;  
National Center for Theoretical Sciences  
National Taiwan University  
No. 1, Sec. 4, Roosevelt Road  
Taipei, Taiwan

\*\*

Institut für Mathematik  
Freie Universität Berlin  
Arnimallee 3  
14195 Berlin, Germany

\*\*\*

Department of Mathematics  
National Taiwan University  
No. 1, Sec. 4, Roosevelt Road,  
10617 Taipei, Taiwan

## Abstract

The celebrated 1975 *Kuramoto model* of  $N$  oscillators with phase angle vector  $\boldsymbol{\vartheta} = (\vartheta_1, \dots, \vartheta_N)$ , frequencies  $\omega_j \in \mathbb{R}$ , and all-to-all coupling constant  $K > 0$  reads

$$(1) \quad \dot{\vartheta}_j = \omega_j + \frac{K}{N} \sum_{k=1}^N \sin(\vartheta_k - \vartheta_j).$$

The model is highly accessible to rigorous mathematical analysis, and has been studied as a paradigm for effects like total and partial synchronization.

In the case of identical frequencies  $\omega_j = \omega$ , we pass to co-rotating coordinates and normalize the time scale in (1) to

$$(2) \quad \dot{\vartheta}_j = \frac{1}{N} \sum_{k=1}^N \sin(\vartheta_k - \vartheta_j).$$

Most initial conditions  $\boldsymbol{\vartheta}$  lead to total synchronization. The plethora of  $2^N - 1$  (circles of) partially synchronized states, however, is unstable. Their precise global rule in transition to synchrony, however, seems to have eluded description.

In the present paper, we address this gap. By the gradient structure of (2), the global dynamics decompose into equilibria and heteroclinic orbits between them. Except for the extremes of total instability and total synchrony, all equilibria are 2-cluster solutions: their phase angles  $\vartheta_j$  attain only two values, with a phase difference of  $\pi$  between them.

Any heteroclinic orbit between 2-cluster equilibria, or towards synchrony, can be realized as a 3-cluster rebellion. The rebellion splits the smaller, “slim”, minority cluster of the source equilibrium and sends the rebellious part to join the bigger, “fat”, majority cluster. This identifies the heteroclinic *connection graph* among 2-cluster equilibria, and towards synchrony, as the lattice of fat index sets, partially ordered by inclusion.

All heteroclinic orbits are in fact geometrically transverse. This identifies the normalized Kuramoto model as a structurally stable Morse–Smale system. In particular, heteroclinic orbits can be concatenated in finite time. The options involved in successive rebellious splittings amount to finite symbol sequences of 2-shift type. Moreover, the connection graph persists for any small deviations from the totally symmetric Kuramoto paradigm.

## Contents

<b>1</b>	<b>Introduction</b>	<b>1</b>
<b>2</b>	<b>Main results</b>	<b>5</b>
<b>3</b>	<b>Partitioned Coordinates</b>	<b>15</b>
<b>4</b>	<b>Stable and unstable manifolds</b>	<b>17</b>
<b>5</b>	<b>Three-cluster orbits</b>	<b>19</b>
<b>6</b>	<b>Transversality</b>	<b>23</b>
<b>7</b>	<b>Numerical solutions</b>	<b>24</b>
<b>8</b>	<b>Discussion</b>	<b>27</b>
8.1	Transients and perturbations . . . . .	27
8.2	Comparison with Stuart–Landau oscillators . . . . .	28

## List of Figures

2.1	Left and right rebellions . . . . .	7
2.2	Concatenation of rebellions I . . . . .	8
2.3	Concatenation of rebellions II . . . . .	11
2.4	Connection graph of five oscillators . . . . .	13
2.5	Swarming rebellion . . . . .	15
5.1	Fundamental triangles of 3-cluster dynamics . . . . .	20
5.2	Fundamental parallelogram of 3-cluster dynamics . . . . .	22
8.1	Concatenations of Stuart–Landau rebellions . . . . .	29

# 1 Introduction

More than 50 years ago, Kuramoto introduced his now classical model of  $N$  oscillators in a famous 3-page proceedings note [Kur75]; see also [Kur84, section 5.4]. With phase angles  $\boldsymbol{\vartheta} = (\vartheta_1, \dots, \vartheta_N)$  on the  $N$ -torus  $\mathbb{T}^N = (\mathbb{R}/2\pi\mathbb{Z})^N$ , frequencies  $\omega_j \in \mathbb{R}$ , and all-to-all coupling constant  $K > 0$ , the *Kuramoto model* reads

$$(1.1) \quad \dot{\vartheta}_j = \omega_j + \frac{K}{N} \sum_{k=1}^N \sin(\vartheta_k - \vartheta_j),$$

for  $j = 1, \dots, N$ . The model has been designed towards accessibility by rigorous mathematical analysis. Therefore, and for its broad applied relevance, it has widely been studied as a paradigm for effects like total and partial synchronization. Google scholar attests to more than 2,500 citations for [Kur75] alone, and more than 10,000 for [Kur84]. In the continuum limit  $N \rightarrow \infty$ , the celebrated results by Chiba [Chib15] have established *phase transition*, away from unique stable distributions, under sufficiently large perturbations of homogeneous frequency distributions. The partial synchronization phenomenon of *chimeras* is widely studied in variants of (1.1), and has originally been discovered in a complex Ginzburg–Landau setting under mean field coupling [KurB02]. For broader surveys see also [Str03, ABP05, PiRo15] and the many references there. A neat web app illustration is [BroStr18].

Our focus, in contrast, is on elucidating qualitative details of transients towards synchronization, for  $N < \infty$ . We mainly address the simplest case of identical frequencies  $\omega_j = \omega$ . This allows us to pass to co-rotating coordinates and normalize the coupling constant  $K$  in (1.1) to

$$(1.2) \quad \dot{\vartheta}_j = \frac{1}{N} \sum_{k=1}^N \sin(\vartheta_k - \vartheta_j).$$

Depending on context, here and below, we use the same notation for angle vectors  $\boldsymbol{\vartheta}$  in  $\mathbb{T}^N$  and in the covering space  $\mathbb{R}^N$ . Most initial conditions  $\boldsymbol{\vartheta}$  lead to total synchronization; see for example [DoXu13, HKP15]. The plethora of partially synchronized states, however, which rule the detailed transition to synchrony, seem to have eluded detailed description. Our main objective will be to address this gap.

Several features of the normalized Kuramoto model (1.2) assist a global description of the dynamics. *Equivariance* under the direct product group

$$(1.3) \quad G = S_N \times \mathbb{S}^1$$

of permutations  $\sigma \in S_N$  of the oscillators, and uniform shifts of all angles  $\vartheta_j$  by  $\psi \in \mathbb{S}^1$ , is the first such feature. Rewriting (1.2) in vector form as

$$(1.4) \quad \dot{\boldsymbol{\vartheta}} = \mathbf{f}(\boldsymbol{\vartheta}),$$

the vector field  $\mathbf{f}$  becomes  $G$ -equivariant. In other words, define the action of  $g = (\sigma, \psi) \in G$  on  $\boldsymbol{\vartheta} \in \mathbb{T}^N$  by

$$(1.5) \quad (g\boldsymbol{\vartheta})_{\sigma(j)} := \vartheta_j - \psi.$$

Then  $\mathbf{f}$  commutes with the action of  $\sigma \in S_N$ , and

$$(1.6) \quad \mathbf{f}(g\boldsymbol{\vartheta}) = \sigma \mathbf{f}(\boldsymbol{\vartheta}),$$

for all  $g = (\sigma, \psi) \in G$  and  $\boldsymbol{\vartheta} \in \mathbb{T}^N$ . Equivalently, this expresses the fact that  $g\boldsymbol{\vartheta}(t)$  solves the Kuramoto model (1.2) whenever  $\boldsymbol{\vartheta}(t)$  does. The action of  $\psi \in \mathbb{S}^1$  is *free*: and  $\boldsymbol{\vartheta}$  is only fixed by  $\psi = 0$ . The action of  $\sigma \in S_N$  is linear on the *covering space*  $\boldsymbol{\vartheta} \in \mathbf{X} = \mathbb{R}^N$  of  $\mathbb{T}^N$ . For some of the enormous local and global consequences of equivariance on dynamics see for example [Van82, Fie88, GoStSch88, ChoLau00, GoSt02] and the references there. For  $S_N$ -equivariance and coupled oscillator settings including Ginzburg–Landau scenarios, more specifically, see also [Elm01, DiSt03, StElCo03, Elm04, KFHK20, FKHK21, GoSt23]. As a curiosity of the co-rotating normalized Kuramoto model (1.2), we mention equivariance under reflections  $\boldsymbol{\vartheta} \mapsto -\boldsymbol{\vartheta}$ , which is hidden in the original setting (1.1). This extends equivariance (1.3) under  $G = S_N \times \mathbb{S}^1$  to the group

$$(1.7) \quad G = S_N \times \mathbb{O}(2).$$

The time-invariance of *cluster subspaces* is an immediate consequence of equivariance. In fact, the linear space of all  $\boldsymbol{\vartheta}$  which are fixed under any particular subgroup of  $S_N$  is time-invariant under (1.4). To choose a subgroup which defines clusters, let

$$(1.8) \quad \{1, \dots, N\} = J_1 \dot{\cup} \dots \dot{\cup} J_M$$

denote any partition  $\mathbf{J} = (J_m)$  into nonempty disjoint index sets  $J_m$  for  $m = 1, \dots, M$ . Let  $S_{\mathbf{J}} = S_{J_1} \times \dots \times S_{J_M}$  denote those permutations  $\sigma$  which only permute elements of each  $J_m$ , separately. In other words,  $S_{\mathbf{J}}$  respects the partition  $\mathbf{J}$  in (1.8). Then the subspace  $\mathbf{X}^{\mathbf{J}}$  of  $\boldsymbol{\vartheta}$  which remain fixed under the group  $S_{\mathbf{J}}$  consists of those vectors  $\boldsymbol{\vartheta}$  which are constant, separately on each index set  $J_m$ , i.e.

$$(1.9) \quad \vartheta_j = x_m, \quad \text{for all } j \in J_m.$$

We call the reduced coordinate vector  $(x_1, \dots, x_M) \in \mathbf{X}^{\mathbf{J}} \cong \mathbb{R}^M$  an *M-cluster*. Let  $N_m$  denote the sizes of the cluster  $J_m$  and abbreviate their size fractions as  $\alpha_m := N_m/N > 0$ . Note  $\sum_{m=1}^M \alpha_m = 1$ . The *M-cluster* dynamics of the Kuramoto model (1.2) on the time-invariant *M-cluster* subspace  $\mathbf{X}^{\mathbf{J}}$  then reads

$$(1.10) \quad \dot{x}_m = \sum_{m'=1}^M \alpha_{m'} \sin(x_{m'} - x_m).$$

Although all  $\alpha_m$  are rational, with shared denominator  $N$ , we may just as well discuss (1.10) for real  $\alpha_m > 0$ . The original case  $M = N$  of single-oscillator *N*-“clusters”  $J_m = \{m\}$ , of course, is subsumed in the above notation. Then  $x_j = \vartheta_j$  with  $\alpha_m = 1/N$ ,  $S_{\mathbf{J}} = \{\text{id}\}$ ,  $\mathbf{X}^{\mathbf{J}} = \mathbf{X} := \mathbb{T}^N$ , and no “clustering” at all.

It is easy to eliminate the free  $\mathbb{S}^1$ -action of  $\psi \in \mathbb{S}^1$ . Indeed, the Kuramoto model (1.2) implies the conservation law  $\sum_{j=1}^N \dot{\vartheta}_j = 0$ . We can therefore use  $\mathbb{S}^1$ -equivariance to reduce all considerations to the linear time-invariant subspace  $\boldsymbol{\vartheta} \in \Xi \cong \mathbb{R}^{N-1}$ , covering an  $(N-1)$ - or  $(M-1)$ -torus

$$(1.11) \quad 0 = \frac{1}{N} \sum_{j=1}^N \vartheta_j = \sum_{m=1}^M \alpha_m x_m.$$

Here we have assumed equality (1.9) of all angles which belong to the same cluster  $J_m$ . For the most elementary example, consider 2-clusters  $M = 2$ . Then (1.10) reads

$$(1.12) \quad \begin{aligned} \dot{x}_1 &= \alpha_2 \sin(x_2 - x_1), \\ \dot{x}_2 &= \alpha_1 \sin(x_1 - x_2). \end{aligned}$$

Without loss of generality, we label size fraction  $\alpha_m$  such that  $0 < \alpha_2 \leq \alpha_1 < 1$ . Normalization (1.11) focuses attention to the time-invariant line

$$(1.13) \quad x_2 = -\alpha_2^{-1} \alpha_1 x_1$$

of rational slope  $-N_1/N_2$ . Passing to angles  $(x_1, x_2) \in \mathbb{T}^2$ , rational slope implies periodicity of the dynamics on the line, with fundamental domain given by the interval  $0 \leq x_2 - x_1 \leq 2\pi$ . Indeed, the end points  $x_2 = x_1$  and  $x_2 = x_1 + 2\pi$  mark exponentially attracting, synchronous 1-cluster equilibria  $\vartheta \equiv \Theta_0 = 0 \bmod 2\pi$ . The midpoint  $x_2 = x_1 + \pi$  of the fundamental interval identifies the unique stationary 2-cluster  $\vartheta \equiv \Theta_- \neq 0 \bmod 2\pi$ . Each half of the fundamental interval consists of a heteroclinic orbit from the exponentially repelling 2-cluster equilibrium  $\Theta_-$  to total synchrony  $\Theta_0$ . Trivial as this 2-cluster dynamics may appear, it will become an important ingredient of our global 3-cluster analysis; see proposition 1.1 and section 5.

A second general feature of the Kuramoto model (1.2) is the *gradient structure*; compare for example [vHeWre93]. This is manifested in the *order parameter*  $R \geq 0$  and  $\Psi \in \mathbb{S}^1$  which are defined as polar coordinates of the averages, alias mean fields

$$(1.14) \quad R \exp(i\Psi) := \frac{1}{N} \sum_{k=1}^N \exp(i\vartheta_k) = \sum_{m=1}^M \alpha_m \exp(ix_m).$$

Here we have already subsumed any  $M$ -cluster case. Multiplication by  $\exp(i\Psi)$  and comparison of real and imaginary parts yields

$$(1.15) \quad R = \frac{1}{N} \sum_{k=1}^N \cos(\vartheta_k - \Psi) = \sum_{m=1}^M \alpha_m \cos(x_m - \Psi);$$

$$(1.16) \quad 0 = \frac{1}{N} \sum_{k=1}^N \sin(\vartheta_k - \Psi) = \sum_{m=1}^M \alpha_m \sin(x_m - \Psi).$$

Multiplication of (1.14) by  $\exp(-i\vartheta_j)$  and comparison of the resulting imaginary parts with (1.2) reveals

$$(1.17) \quad \dot{\vartheta}_j = R \sin(\Psi - \vartheta_j),$$

for all  $j$ . In view of clustering (1.9), of course, we may as well substitute  $\vartheta_j$  by  $x_m$  here. To determine  $\dot{R}$ , we differentiate (1.15) along solutions. Eliminating  $\dot{\Psi}$  by (1.16) provides the gradient structure

$$(1.18) \quad \dot{R} = R \cdot \frac{1}{N} \sum_{k=1}^N \sin^2(\Psi - \vartheta_k) = R \cdot \sum_{m=1}^M \alpha_m \sin^2(\Psi - x_m) \geq 0$$

with the order parameter  $R \geq 0$  as a *nondecreasing Lyapunov function*.

Note that  $\dot{R}$  vanishes at equilibria  $\vartheta \equiv \Theta$ , only. In fact, the set  $\{\Theta \in \Xi \mid R = 0\}$  consists of equilibria  $\vartheta_j \equiv \Theta_j$ , by (1.17). For  $R > 0$ ,  $\dot{R} = 0$  in (1.18) implies  $\sin(\Psi - \vartheta_j) = 0$ , for all  $j$ . Again, (1.17) implies we are at equilibrium. Moreover, the vanishing sine implies  $\vartheta_j \equiv \Theta_j \in \{\Psi, \Psi + \pi\}$  can attain at most two values. Therefore,  $\Theta$  is either a synchronous 1-cluster equilibrium, at  $R = 1$ , or a 2-cluster equilibrium, at  $0 < R = 2\alpha - 1 < 1$ . Indeed,  $M = 2$  and  $\alpha_1 + \alpha_2 = 1$  imply  $0 < \alpha_2 < 1/2 < \alpha_1$ , without loss of generality. We choose  $\alpha = \alpha_1 = N_1/N > 1/2$  to indicate the *fat cluster* of size  $N_1 > N/2$  at  $x_1 = (\alpha - 1)\pi$ . The *slim cluster* of complementary size  $N_2 = N - N_1 < N/2$  is located at  $x_2 = \alpha\pi$ , by the phase constraint (1.11). The symmetric case  $\alpha_1 = \alpha_2 = 1/2$  leads to  $R = 0$  and is subsumed under the following remarks.

By (1.14), the equilibria satisfying  $R = 0$  define *closed planar  $N$ -bar linkages*, a ubiquitously important device in mechanical engineering. In the complex plane, the length of each joint is 1, and the directional angles are  $\vartheta_j$ . General  $M$ -bar linkages with rational joint lengths occur as  $M$ -cluster variants, and we may easily generalize to include real lengths. The linkages need not be convex  $N$ -gons, and may even intersect themselves. See the monograph [McCSoh11] for a wealth of fascinating details from an engineering point of view.

A neighborhood of sufficiently small  $R > 0$  can elegantly be studied via a Möbius transform of coordinates, which are called Watanabe–Strogatz variables; for applications see for example [PiRo09] and the survey [PiRo15]. Unfortunately, these variables do not cover the whole phase space. For example, the required normalization  $\sum \exp(i\xi_j) = 0$ , in their notation, misses any 2-cluster equilibrium with order parameter  $R > 0$ . Indeed, equal cluster-angles  $\vartheta_j = x_m$  lead to equal  $\xi_j$ , and clustering with  $\alpha_1 > 1/2 > \alpha_2$  contradicts the required Watanabe–Strogatz normalization.

We summarize our preliminary observations on equilibria in the following proposition.

**1.1 Proposition** (Classification of equilibria). *The equilibria  $\vartheta = \Theta$  of the Kuramoto model (1.2) fall into three classes. Under the angle normalization (1.11), the three classes can be characterized by decreasing order parameter  $R$  and decreasing stability as follows:*

- (i)  $R = 1$ : the totally stable circle of synchronous equilibria, represented by  $\Theta = 0$ ;
- (ii)  $0 < R = 2\alpha - 1 < 1$ : the normally hyperbolic circles of 2-cluster equilibria  $\Theta$  of strong unstable dimension  $i = N_2$ , with fat and slim size fractions  $1/2 < \alpha = \alpha_1 = N_1/N < 1$  and  $0 < \alpha_2 = 1 - \alpha < 1/2$ , represented in the fundamental domain of  $0 \leq x_2 - x_1 \leq 2\pi$  by the mid-point  $x_1 = (\alpha - 1)\pi$ ,  $x_2 = \alpha\pi$ ; see (1.12) and (1.13);
- (iii)  $R = 0$ : the totally unstable closed planar  $N$ -bar linkages  $\sum_{j=1}^N \exp(i\Theta_j) = 0$  of unit joint lengths, rotated such that  $\sum_{j=1}^N \Theta_j = 0$  is normalized.

At any given critical level  $0 < R = 2\alpha - 1 < 1$ , we encounter  $\binom{N}{\alpha N} = \binom{N}{N_1}$  distinct circles of 2-cluster equilibria. The cases correspond to the partitions of  $\{1, \dots, N\}$  into nonempty complementary index sets  $J_1 = J$  and  $J_2 = J^c$  of sizes  $N_1 = \alpha N$  and  $N_2 = (1 - \alpha)N$ , respectively. Proposition 1.1 will be proved in section 3. The (in-)stability claims (i) and (iii) follow from the Lyapunov property (1.18) and the absence of further equilibria near  $R = 1$  and  $R = 0$ , respectively.

By the Lyapunov function  $R$  and normal hyperbolicity, non-equilibrium solutions  $\vartheta(t)$  become heteroclinic between distinct equilibria  $\Theta_{\pm}$ , for  $t \rightarrow \pm\infty$ . In symbols,

$$(1.19) \quad \vartheta_*(t) : \quad \Theta_- \rightsquigarrow \Theta_+ \neq \Theta_-.$$

The only exception are  $N$ -bar linkage source equilibria  $\Theta_-$ , for which we cannot assert backwards convergence to a single equilibrium, but only convergence to the equilibrium set  $\{\Theta \in \Xi \mid R = 0\}$ . Henceforth, we only address heteroclinicity among 1- and 2-cluster equilibria  $\Theta_{\pm}$  with  $R > 0$ , including convergence to the 1-cluster equilibria  $R = 1$  of total synchrony. We factor out the  $\mathbb{S}^1$ -action of the equivariance group  $G$  by the angle normalization (1.11). This picks a single representative for each equilibrium circle, hyperbolic for  $R > 0$ . The *connection graph* will consist of these equilibria, as vertices, and edges which represent the sets of rebellious heteroclinic orbits (1.19) between equilibria. See corollary 2.7. We occasionally include  $R = 0$  as a single top vertex.

The paper is outlined as follows. In the next section, we collect our main results. Specifically, theorem 2.1 establishes necessary relations among the source equilibrium  $\Theta_-$  and target equilibrium  $\Theta_+$ , for any heteroclinic edge in the connection graph. The more elementary aspects (i) and (ii) of theorem 2.1 are proved right there. Theorem 2.2 then shows how any heteroclinic edge can already be realized by a rebellious 3-cluster heteroclinic orbit, which splits the slim 2-cluster of the source  $\Theta_-$ . Theorem 2.4 establishes transversality, in full space, of general heteroclinic orbits which need not be 3-clusters. In corollaries 2.5–2.8, we collect some consequences of these results. In particular, we observe structural stability, for  $R > 0$ , and transitivity of the connection graph. Theorem 2.9 characterizes general heteroclinic rebellions  $\vartheta_*(t) : \Theta_- \rightsquigarrow \Theta_+$  and their realization by multi-cluster swarms.

Section 3 introduces *partitioned coordinates* for a deeper analysis of the interplay between 3-cluster heteroclinicity and general perturbations of initial conditions. The proof of proposition 1.1 on 2-cluster equilibria is an immediate illustration. In section 4, clustered coordinates provide a global description of stable and unstable manifolds. In particular, lemma 4.2(ii) proves theorem 2.1(iii) on monotonicity of fat clusters. Theorem 2.2 on 3-cluster realization of heteroclinic orbits is proved in section 5, and transversality theorem 2.4 follows in section 6. For comments on the numerical illustrations of our results see section 7. We conclude with a discussion, as outlined at the beginning of section 8.

**Acknowledgment.** We are grateful to Chien-Yu Chen for pointing out the connection problem between partially synchronous equilibria. Jia-Yuan Dai was supported by NSTC (National Science and Technology Council) grant 113-2628-M-007-005-MY4. Alejandro López-Nieto has been supported by NSTC grant 113-2123-M-002-009. Jia-Yuan Dai and Bernold Fiedler are indebted for mutual hospitality during in-person working visits, and the pertinent grant support.

## 2 Main results

In this section we formulate our main results on the global dynamics of the Kuramoto model (1.2). We consider heteroclinic orbits  $\vartheta(t) : \Theta_- \rightsquigarrow \Theta_+$  among synchronous 1-cluster and 2-cluster equilibria  $\Theta_{\pm}$  at levels  $0 < R_- < R_+ \leq 1$  of the order parameter.



See proposition 1.1 and (1.19). Theorem 2.1 collects necessary conditions for such heteroclinic rebellions. Based on these conditions, theorem 2.2 shows that, conversely, general heteroclinic connections can be represented by 3-cluster variants. Theorem 2.4 establishes transversality of general heteroclinic orbits. Corollaries 2.6–2.8 collect some consequences for the connection graph and concatenation of heteroclinic rebellions. Theorem 2.9 addresses general multi-cluster heteroclinic swarms. Throughout, and without loss of generality, we eliminate  $\mathbb{S}^1$  shift-equivariance by the time-invariant angle normalization (1.11).

**2.1 Theorem** (Angles and monotonicity of equilibrium 2-clusters). *Consider any non-stationary orbit  $\vartheta(t) \in \mathbb{T}^N$  for  $t \in \mathbb{R}$ , with a positive lower bound  $0 < R_- := \inf_{t \in \mathbb{R}} R(t)$  of the Lyapunov order parameter  $R$  on the orbit. Then  $\vartheta(t)$ :  $\Theta_- \rightsquigarrow \Theta_+$  is heteroclinic between two equilibria  $\Theta_{\pm}$  with order parameters  $0 < R_- < R_+ \leq 1$ . Moreover,*

- (i)  $\Theta_{\pm}$  are either 1- or 2-cluster equilibria with size fractions  $1/2 < \alpha_{\pm} = (R_{\pm} + 1)/2 \leq 1$  of the fat clusters  $\alpha_1 = \alpha_{\pm} = N_{1,\pm}/N$  supported on index sets  $J_1 = J_{\pm}$ , respectively;
- (ii) the phase angles  $x_1 = x_{\pm}$  of the fat clusters are represented by  $x_{\pm} = (\alpha_{\pm} - 1)\pi$ ;
- (iii) the fat clusters are supported on strictly growing index sets  $J_+ \supsetneq J_-$ .

The exceptional case  $\Theta_+ = 0$  of a totally synchronous target 1-cluster is subsumed here as  $R_+ = \alpha_+ = 1$ .

**Proof of claims (i) and (ii).** Convergence to equilibria follows from relative compactness of the orbit  $\vartheta(t) \in \mathbb{T}^N$ , the Lyapunov property (1.18), and the LaSalle invariance principle. Convergence to single equilibria follows from  $0 < R_- < R_+$  and their hyperbolicity after elimination of phase shifts by (1.11). See proposition 1.1(i)–(ii), which also prove the remaining parts in claims (i)–(ii) of the theorem.  $\square$

Claim (iii) on monotonicity of fat clusters will be proved in lemma 4.2. This claim is somewhat surprising: once a cluster has gained absolute majority  $\alpha_- > 1/2$  of its supporters  $J_-$ , it will never lose any of its adherents by later rebellion. Rather, rebels only break up the slim minority cluster  $J_-^c = J_2 \dot{\cup} J_3$ , by rebellion towards the fat majority cluster.

We now assert that, conversely, all heteroclinicity with  $\inf_{t \in \mathbb{R}} R(t) > 0$  is realized, either by a 3-cluster heteroclinic orbit between 2-cluster equilibria, or else by a 2-cluster heteroclinic orbit towards synchrony.

**2.2 Theorem** (Realization of 3-cluster heteroclinic orbits). *Let  $\Theta_{\pm}$  denote any two equilibria with order parameters  $0 < R_- < R_+ < 1$ . Assume that the index sets  $J_{\pm}$  of their fat clusters satisfy  $J_- \subsetneq J_+$  and  $J_+^c \neq \emptyset$ . Then there exists a 3-cluster heteroclinic orbit  $\vartheta_*(t)$ :  $\Theta_- \rightsquigarrow \Theta_+$ .*

More precisely, the above pairs  $\Theta_{\pm}$  of 2-cluster equilibria are in one-to-one correspondence to certain index partitions (1.8) by  $J_1 \dot{\cup} J_2 \dot{\cup} J_3$  with size fractions  $0 < \alpha_2, \alpha_3 < 1/2 < \alpha_1 < 1$  of cluster sizes  $N_1 + N_2 + N_3 = N$ . Specifically,

$$(2.1) \quad \begin{aligned} J_1 &= J_- , & J_2 &= J_+ \setminus J_- , & J_3 &= J_+^c , \\ \alpha_1 &= \alpha_- , & \alpha_2 &= \alpha_+ - \alpha_- , & \alpha_3 &= 1 - \alpha_+ ; \end{aligned}$$

see theorem 2.1. Let  $(x_1, x_2, x_3)$  denote 3-cluster coordinates (1.9) with angle normalization (1.11), i.e.  $\alpha_1 x_1 + \alpha_2 x_2 + \alpha_3 x_3 = 0$ . Since the cluster angles  $x_m(t)$  for  $m = 1, 2, 3$

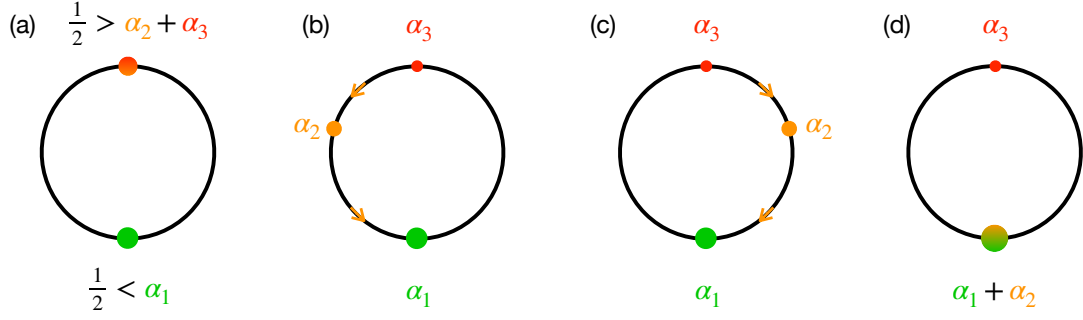


**Figure 2.1:** Heteroclinic left and right 3-cluster rebellions  $\vartheta_*(t)$ :  $\Theta_- \rightsquigarrow \Theta_+$ ; see theorem 2.2. Antipodal angles  $x_1 = x_-$  (green) and  $x_2 = x_3 = x_- + \pi$  (red) of the 2-cluster source equilibrium  $\Theta_-$  and the target equilibrium  $\Theta_+$  are marked by solid dots on the phase circle  $\mathbb{S}^1$ , in (a) and (d). Areas of dots refer to cluster size.

In (b) and (c): heteroclinic rebellions of cluster  $x_2$  (orange), which splits off from the slim cluster at  $x_2 = x_3$  to join the fat cluster at  $x_2 = x_1$ . See (2.1) and (2.2), respectively. Left rebellion of cluster  $x_2$  is illustrated in (b), and right rebellion in (c); see (2.3)–(2.4). Cases (b) and (c) are interchanged under reflections (1.7).

cannot cross, for finite  $t$ , their order relation must be preserved. Consider the fundamental region  $x_1 \leq x_2, x_3 \leq x_1 + 2\pi$ .

Then the 3-cluster heteroclinic orbit  $\vartheta_*(t)$  is supported on the index partition (2.1) associated to  $\Theta_{\pm}$ . Whereas  $\lim x_1(t) = x_{\pm}$  and  $\lim x_3(t) = x_{\pm} + \pi$ , for  $t \rightarrow \pm\infty$ , the phase  $x_2(t)$  of the rebel cluster  $J_2$  switches allegiance:

$$(2.2) \quad \lim x_2(t) = \begin{cases} x_- + \pi, & \text{for } t \rightarrow -\infty, \\ x_+, & \text{for } t \rightarrow +\infty. \end{cases}$$

The following alternatives are each realized by 3-cluster heteroclinic orbits  $\vartheta_*$ :

$$(2.3) \quad x_1 < x_3 < x_2 < x_1 + 2\pi \quad \text{and}$$

$$(2.4) \quad x_1 < x_2 < x_3 < x_1 + 2\pi.$$

See figure 2.1, where we call case (2.3) a left rebellion (b), and case (2.4) a right rebellion (c), respectively.

In the case  $R_+ = 1$  of convergence towards total synchrony  $\Theta_+ = 0$  and  $J_+^c = \emptyset$ , the heteroclinic orbit  $\vartheta_*(t)$  can be chosen to be of 2-cluster type.

See figure 2.2 for an illustration of successive one-man rebellions  $\alpha_2 = 1/N$  and their influence on the cluster positions  $x_1, x_3$ . Here  $x_1 = x_1(t)$  keeps track of the angles  $\vartheta_j$  of  $j \in J_-$ , and  $x_3$  refers to  $j \in J_3 = J_+^c$ ; see (2.1). To track the rebel position  $x_2(t)$ , we define the shift symbols

$$(2.5) \quad s = \begin{cases} -, & \text{for a left rebellion,} \\ +, & \text{for a right rebellion,} \end{cases}$$

as in figure 2.1(b), (c), respectively.

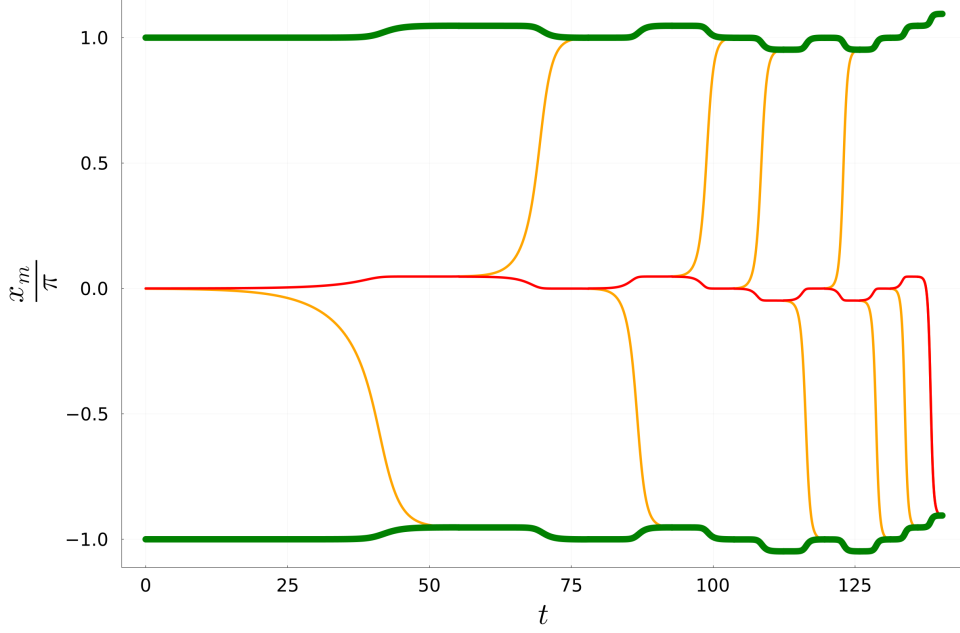


**Figure 2.2:** Time plot of  $n = 10$  successive one-man rebellions towards synchrony, concatenated to a heteroclinic orbit  $\Theta_*(t)$ :  $\Theta_0 \rightsquigarrow \Theta_n$ . The three cluster phases (vertical) are  $x_1$  (fat, green),  $x_2$  (one-man rebellions  $N_2 = 1$ , orange) and  $x_3$  (slim, red) 3-cluster rebellions. Compare figure 2.1 for side-switching of the rebellions. Initial cluster sizes are  $N_1 = 11$ ,  $N_2 = 1$ ,  $N_3 = 9$  for  $N = 21$  oscillators, with phases near equilibrium  $x_1/\pi = \alpha_1 - 1 = -10/21$  and  $x_2/\pi = x_3/\pi = \alpha_1 = 11/21$ , for  $t \rightarrow -\infty$ . Thickness of trajectories refers to cluster size. Note the nine successive one-man transients (orange) of faster and faster ejection from the slimming red cluster, and convergence to the fattening green cluster. Left transients, as in figure 2.1(b) appear above the red graph of slim  $x_2(t)$ , and right transients 2.1(c) appear below. In symbols (2.23),  $s = + - + - - + - + +$ . The final tenth “transient” (red, down) vacates the final near-antipodal red slim “cluster” of “last man standing” opposition, entirely, and achieves synchrony, at last. See [Fie94, AOWT07, KGO15] and figure 8.1 below for related ideas. Note how each one-man rebellion  $s_\ell = \pm$  induces parallel drifts by  $s_\ell \alpha_2 \pi = \pm \pi/N$  in the position  $x_1$  of the fat majority cluster. See corollary 2.3.

**2.3 Corollary** (Phase shifts). Consider any 3-cluster heteroclinic orbit  $\vartheta_*(t)$ :  $\Theta_- \rightsquigarrow \Theta_+$  as in theorem 2.2. Then the heteroclinic rebellion of  $x_2(t)$  causes a shift of  $x_1(t)$  for  $t \rightarrow \pm\infty$  by

$$(2.6) \quad x_1(+\infty) - x_1(-\infty) = s \alpha_2 \pi,$$

and similarly for the limits  $x_3(\pm\infty) = x_1(\pm\infty) + \pi$ .

**Proof.** In the limit  $t \searrow -\infty$ , we obtain

$$(2.7) \quad x_- := x_1(-\infty) = (\alpha_1 - 1)\pi,$$

$$(2.8) \quad x_3(-\infty) = \alpha_1 \pi.$$

Here we have used proposition 1.1(ii) and theorem 2.1(ii). In the limit  $t \nearrow +\infty$ , the phase normalization (1.11) for angles  $\vartheta_j(t) \in J_m$  implies

$$(2.9) \quad 0 = \alpha_1 x_+ + \alpha_2 x_2(+\infty) + \alpha_3 (x_+ + \pi).$$

The orders (2.3), (2.4) of left and right rebellions imply

$$(2.10) \quad x_2(+\infty) = x_1(+\infty) + (1-s)\pi = x_+ + (1-s)\pi.$$

Substitution of (2.10) and (2.7) into (2.9) with  $\alpha_1 + \alpha_2 + \alpha_3 = 1$  then proves claim (2.6), and the corollary.  $\bowtie$

The alert reader may notice, that a left rebellion  $s = -$  violates the condition (1.9) in cluster  $J_1$  at the target equilibrium  $\Theta_+$ . Indeed (2.10) then forces a discrepancy of  $2\pi$  among  $\vartheta_j$  of the fat cluster  $J_+ = J_- \cup J_2$ . As long as  $x_1$  keeps track of  $\theta_j$  in  $J_1$ , only, this will not interfere with concatenation of transitions, in corollary 2.6 below. The phase normalization (1.11) as used in the above proof, however, will only hold if we include  $j \in J_2$  in the summation of angles.

Next we address transversality of stable and unstable manifolds along arbitrary heteroclinic orbits  $\vartheta_*(t)$ :  $\Theta_- \rightsquigarrow \Theta_+$  with  $0 < R_- < R_+ \leq 1$ . As usual, we subsume the synchronous 1-cluster equilibrium  $\Theta_+ = 0$  at  $R = 1$  here. Let  $W_-^s$  and  $W_+^u$  denote the stable and unstable manifolds, respectively, of the two hyperbolic equilibria  $\Theta_\pm$ , in the space  $\vartheta \in \Xi \cong \mathbb{R}^{N-1}$  of angle normalization (1.11). For some general background on invariant manifolds see for example [ChoHa82, PdM82]. Any heteroclinicity  $\vartheta_*(t)$ :  $\Theta_- \rightsquigarrow \Theta_+$  is equivalent to a nonempty intersection

$$(2.11) \quad \vartheta_*(t) \in W_-^u \cap W_+^s.$$

We say that  $W_-^u$  and  $W_+^s$  are *transverse*, or *intersect transversely*, along the heteroclinic orbit  $\vartheta_*(t) \in \Xi$ , if the sum of their tangent spaces spans all of  $\Xi$ , i.e.,

$$(2.12) \quad T_{\vartheta_*(t)}W_-^u + T_{\vartheta_*(t)}W_+^s = \Xi$$

for some, and hence all,  $t \in \mathbb{R}$ . In symbols, we also express such transversality as

$$(2.13) \quad W_-^u \nparallel_{\vartheta_*(t)} W_+^s \quad \text{or} \quad \Theta_- \overset{\vartheta_*(t)}{\rightsquigarrow} \nparallel \Theta_+.$$

As an immediate consequence of transversality at  $\vartheta_*(t)$ , the time-invariant intersection of the stable and unstable manifolds is itself a manifold, of dimension

$$(2.14) \quad \dim(W_-^u \cap W_+^s) = i_- - i_+ = N_{2,-} - N_{2,+}.$$

Here  $i_\pm = N_{2,\pm}$  denote the *unstable dimensions* or *Morse indices* of the hyperbolic equilibria  $\Theta_\pm$  in  $\Xi$ , respectively. See proposition 1.1(ii). Factoring out the time direction, e.g. by a Poincaré cross section transverse to the flow, this provides a local manifold of heteroclinic orbits of dimension  $i_- - i_+ - 1 \geq 0$ . Transverse heteroclinic orbits between adjacent Morse indices  $i_\pm$ , in particular, are isolated and hence locally unique. Transverse homoclinic orbits, or saddle-saddle connections with  $i_- \leq i_+$ , are excluded, *per se*.

The next theorem asserts transversality, automatically, along heteroclinic orbits.

**2.4 Theorem** (Transverse heteroclinics). *Let  $\vartheta_*(t)$ :  $\Theta_- \rightsquigarrow \Theta_+$  denote any heteroclinic orbit between two equilibria  $\Theta_\pm$  with order parameters  $0 < R_- < R_+ \leq 1$ . Then the stable and unstable manifolds  $W_-^u$  and  $W_+^s$  intersect transversely along  $\vartheta_*(t) \in \Xi$ , i.e.*

$$(2.15) \quad \Theta_- \overset{\vartheta_*(t)}{\rightsquigarrow} \nparallel \Theta_+.$$

The significance of such *transverse heteroclinicity* is two-fold. *First*, transversality in Morse–Smale systems implies  $C^0$  structural stability in compact settings. The *Morse–Smale property* assumes equilibria and periodic orbits as the only recurrence, and with transverse heteroclinicity among them. *Structural stability* then asserts that  $C^1$ -small perturbations lead to  $C^0$  orbit equivalent flows, i.e., flow-orbits are mapped to orbits under a global near-identity homeomorphism. See [Pa69, PaSm70, PdM82, HMO02] for details. For certain perturbations for the Kuramoto model (1.2) see section 8.1.

In co-rotating coordinates (1.2) and under angle normalization (1.11) to the subspace  $\Xi \cong \mathbb{R}^{N-1}$ , viz. the orthogonal projection  $\mathbb{T}^{N-1}$  of  $\mathbb{T}^N$  to  $\Xi$ , we have just established the Morse–Smale property on the positively invariant subset  $\{\vartheta \in \mathbb{T}^{N-1} \mid R(\vartheta) > 0\}$ . For hyperbolicity see proposition 1.1 and theorem 2.1. Theorem 2.4 asserts transversality of all heteroclinic orbits within the *maximal compact invariant* subset  $\mathcal{A}$  of  $\{\vartheta \in \mathbb{T}^{N-1} \mid R(\vartheta) > 0\}$ , commonly called the *global attractor*. For our finite-dimensional setting of the normalized Kuramoto model (1.2) in  $\Xi$ , we borrow this terminology from infinite-dimensional dynamics. The Morse–Smale property of (1.2) then implies Morse–Smale structural stability on  $\mathcal{A}$  in  $\Xi$ . See [HMO02, chapter 6].

In full space  $\mathbb{T}^N$ , however, the equilibria form nonhyperbolic stationary lines, alias circles mod  $2\pi$ . In principle, this violates the Morse–Smale paradigm of structural stability. Nevertheless, once we undo the passage from (1.1) to co-rotating coordinates (1.2), the equilibrium circles revert to their original manifestation as hyperbolic periodic orbits, for  $\omega \neq 0$ . The stable and unstable manifolds of each periodic orbit consist of the union of all stable and unstable manifolds of all its frozen equilibrium cousins. Frozen transversality in  $\mathbb{T}^{N-1}$  lifts to  $\mathbb{T}^N$ , because the constant drift  $\omega t$  increases the dimension of the stable and unstable manifolds by one, each. In particular, the Kuramoto model (1.1) with equal frequencies is Morse–Smale in  $\mathbb{T}^N$  and, therefore, structurally stable for  $R > 0$ . This proves the following corollary.

**2.5 Corollary** (Morse–Smale structural stability). *The classical Kuramoto model (1.1) with identical frequencies  $\omega_j = \omega \neq 0$  is Morse–Smale. The flow on the global attractor  $\mathcal{A}$  of (1.1) within the positively invariant subset  $\{\vartheta \in \mathbb{T}^N \mid R(\vartheta) > 0\}$  is structurally stable under  $C^1$ -small perturbations of the flow.*

We now return to the gradient setting of the co-rotating Kuramoto model (1.2) with angle normalization (1.11). The *second* consequence of transversality theorem 2.15 is *transitivity* of the heteroclinicity relation. More precisely, suppose we have a sequence of transverse heteroclinic orbits

$$(2.16) \quad \Theta_0 \xrightarrow[\overline{\mathfrak{H}}]{\vartheta_1(t)} \Theta_1 \xrightarrow[\overline{\mathfrak{H}}]{\vartheta_2(t)} \dots \xrightarrow[\overline{\mathfrak{H}}]{\vartheta_n(t)} \Theta_n$$

between successive hyperbolic equilibria  $\Theta_0, \dots, \Theta_n$ . Then arbitrarily close to the union of  $\vartheta_\ell(t)$  and their rest stops  $\Theta_\ell$ , there exists a direct transverse heteroclinic orbit

$$(2.17) \quad \Theta_0 \xrightarrow[\overline{\mathfrak{H}}]{\Theta_*(t)} \Theta_n.$$

We call any such  $\Theta_*(t)$  a *concatenation* of the successive heteroclinic steps  $\vartheta_1(t), \dots, \vartheta_n(t)$ . This is a consequence of the  $\lambda$ -Lemma [PdM82]. Actually, Lin’s method provides a refinement: for any sufficiently large  $T_* > 0$ , *passage times*  $T_1, \dots, T_{n-1} \geq T_*$  near the

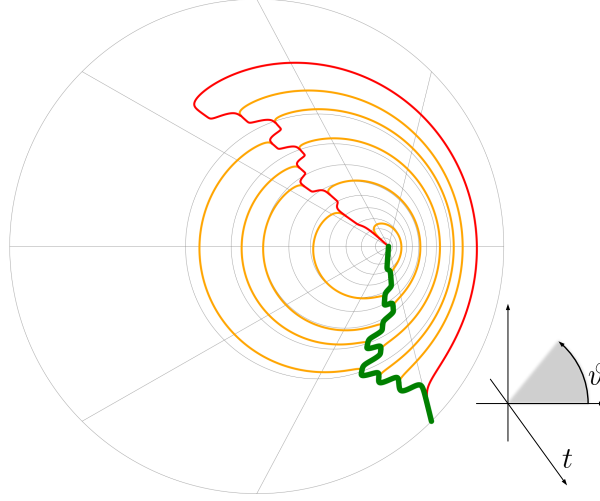


**Figure 2.3:** Phase plots of  $n = 10$  successive side-switching one-man rebellions towards synchrony, concatenated to a heteroclinic orbit  $\Theta_*(t): \Theta_0 \rightsquigarrow \Theta_n$ . The plot is based on the same data as figure 2.2, with the same color coding. Phases  $x_m \in \mathbb{S}^1$  are drawn on a cylinder  $(x_m, t) \in \mathbb{S}^1 \times \mathbb{R}$  with vanishing point of perspective at  $t = -\infty$ . Thin gray lines mark a cylindrically Cartesian grid with angle sectors of width  $\pi/4$ . Clockwise orange transients, right, follow figure 2.1(c). Counter-clockwise orange transients, left, follow figure 2.1(b). Their tangencies point to the front, in the direction of time. The final tenth “transient” (red, right) vacates the final near-antipodal red slim “cluster” of “last man standing” opposition, entirely, and achieves synchrony, at last.

intermediate equilibria  $\Theta_1, \dots, \Theta_{n-1}$  can be prescribed arbitrarily. See [Lin90, Lin08] for details. As a consequence, we obtain the following corollary to theorem 2.4. See figures 2.2–2.3 for illustrations.

**2.6 Corollary** (Concatenation of heteroclinic orbits). *Consider any sequence of 1- and 2-cluster equilibria with ascending order parameters*

$$(2.18) \quad 0 < R(\Theta_0) < \dots < R(\Theta_n) \leq 1.$$

As in (2.16), let  $\vartheta_1(t), \dots, \vartheta_n(t)$  denote any associated sequence of heteroclinic orbits between those equilibria, transverse by theorem 2.4, but not necessarily of 2- or 3-cluster type.

Then there exist direct transverse concatenated heteroclinic orbits

$$(2.19) \quad \Theta_0 \xrightarrow[\overline{\cap}]{\Theta_*(t)} \Theta_n.$$

For  $n \geq 2$ , the concatenations  $\Theta_*(t)$  are not of 3-cluster type.

The converse phenomenon of *cascading* is a consequence of theorems 2.1–2.2, as follows. Consider any two 1- or 2-cluster equilibria  $\Theta_{\pm}$  with Morse indices  $0 \leq i_+ = i_- - n$  and any heteroclinic orbit  $\vartheta_*(t): \Theta_- \rightsquigarrow \Theta_+$  between them. We do not require  $\vartheta_*(t)$  to be of 3-cluster type. The fat clusters of  $\Theta_{\pm}$  are then supported on  $J_+ \supsetneq J_-$ ; see theorem 2.1(iii). Theorem 2.2 then asserts that there exists a 3-cluster heteroclinic orbit  $\vartheta_*(t): \Theta_- \rightsquigarrow \Theta_+$  between the same equilibria.

Next consider any sequence

$$(2.20) \quad J_- = J_0 \subsetneq \dots \subsetneq J_n = J_+$$



of  $n+1$  fat clusters  $J_\ell$ , which strictly ascends by adding one single oscillator, at a time. Let  $\Theta_\ell$  denote the 1- or 2-cluster equilibria with those fat clusters, and note their descending Morse indices

$$(2.21) \quad i_\ell := i(\Theta_\ell) = i_- - \ell.$$

By the same reasoning as above, this induces a sequence (2.16) of  $n$  transverse heteroclinic orbits  $\vartheta_\ell(t)$  with  $J_{\ell-1}$  as fat cluster. Each transverse heteroclinic orbit  $\vartheta_\ell(t)$  increases the size of the fat cluster by 1, and hence is a one-man rebellion with size  $N_2 = 1$  of the rebellious cluster  $J_2$ . Therefore, each one-man rebellion  $\vartheta_\ell(t)$  is a 3-cluster. By transversality (2.14), each rebellion orbit  $\vartheta_\ell(t)$  is isolated. The term “cascading” describes the above “interpolation” phenomenon by a *cascade*  $\vartheta_\ell(t)$  of one-man rebellions, each of which drops the Morse index by 1.

As a caveat, we add that cascading may fail in general Morse systems. The height flow on the standard  $n$ -sphere  $\mathbb{S}^n \subset \mathbb{R}^{n+1}$  is a counterexample. Rather, cascading is a very peculiar feature of the Kuramoto model (1.2). In the technically very different context of scalar one-dimensional PDEs of reaction-drift-diffusion type, cascading has first been observed in [FieRo96]; see also [FieRo20, FieRo23, FieRo24, RFLN25] for later illustrations.

Combining theorems 2.1–2.4, we can describe the *connection graph*  $\mathcal{C}$  of the Kuramoto model (1.2) for order parameters  $0 < R \leq 1$  and under the phase constraint (1.11). By proposition 1.1(i)–(ii), all equilibria  $\Theta_J$  with  $R > 0$  are hyperbolic, and are characterized by their fat cluster set  $J$  of size fraction  $\alpha = N_1/N = (R+1)/2 > 1/2$ . These  $\Theta_J$ , alias  $J$ , serve as the *vertices* of  $\mathcal{C}$ . By the Lyapunov property (1.18), all other orbits  $\vartheta(t)$  which remain in this region of  $0 < R \leq 1$  for all times  $t \in \mathbb{R}$  are heteroclinic among those equilibria. *Edges* of  $\mathcal{C}$  represent such heteroclinicity.

The description of global dynamics by connection graphs has been common in variational settings of Morse type. For many examples involving PDEs with nodal properties see [BrFie88, BrFie89, FieRo96, Rau02, FieRo20, FieRo23, FieRo24, RFLN25] and the references there. See [Con78, FrM88, MM02, KaMM04] for general, not necessarily variational settings related to Conley index. For recent adaptations to general settings of global dynamics see also [DLY24, ADLY25].

**2.7 Corollary** (Connection graph). *The connection graph  $\mathcal{C}$  among the equilibria  $\Theta_J$  with  $R > 0$  is given by the partial order of the fat subsets  $J$  with respect to inclusion, as edges. Heteroclinic orbits orient each edge towards the larger index set  $J$ .*

By cascading, transitivity theorem 2.4, and the resulting transitivity of heteroclinicity, it is sufficient to represent the connection graph by its edges between fat cluster sets  $J$  of adjacent size. Adjoining an artificial vertex  $\mathbf{0}$  to represent the  $N$ -bar linkage equilibrium set  $\{\Theta \in \Xi \mid R = 0\}$ , the connection graph becomes a finite lattice defined by subset inclusion. The number  $V$  of vertices in the lattice is given by

$$(2.22) \quad V = 1 + \sum_{N_1=\lfloor N/2 \rfloor + 1}^N \binom{N}{N_1} = \begin{cases} 2^{N-1} + 1, & \text{for } N \text{ odd,} \\ 2^{N-1} + 1 - \frac{1}{2} \binom{N}{N/2}, & \text{for } N \text{ even.} \end{cases}$$

Here  $N_1 = |J| = \alpha N > N/2$ , and  $\lfloor \cdot \rfloor$  denotes the floor function. See figure 2.4 for the example  $N = 5$ . For abbreviated annotation, we have replaced fat vertex labels  $J$  by

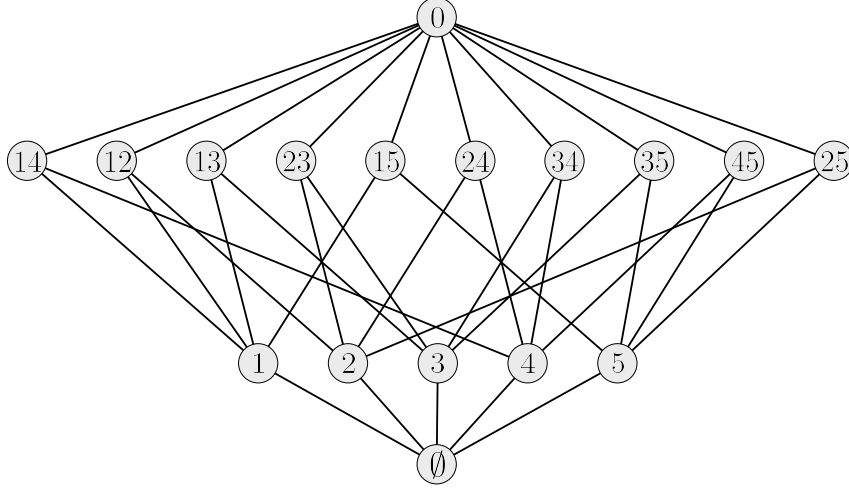


**Figure 2.4:** Connection graph  $\mathcal{C}$  for the Kuramoto model (1.2) with  $N = 5$  oscillators. Equilibrium vertices  $\Theta_J$  are represented by their complementary slim cluster sets  $J^c$  of size  $|J^c| = N_2 = 5 - |J|$ . Note order parameters  $0 < R = 2\alpha - 1 = 1 - 2/5|J^c| \leq 1$ , and Morse indices  $i = |J^c|$ . The 5-bar linkage equilibrium set  $\{\Theta \in \Xi \mid R = 0\}$  is represented by the artificial top vertex 0. The lowest level  $\emptyset$  signifies an empty slim cluster, that is, total synchrony. Directed edges represent heteroclinicity between adjacent Morse levels. In view of cascading and transverse transitivity, directed paths in  $\mathcal{C}$  capture all heteroclinicity. In particular, edges are directed downward, towards lower Morse index  $i$  and larger order parameter  $0 < R \leq 1$ .

their slim complements  $J^c$  there. Heteroclinic orientation is downward, towards increasing order parameter  $R = 2\alpha - 1$  and decreasing Morse index  $i = N_2 = |J^c|$ .

For general  $N$ , we can thus describe the connection graph based on the well-known *subset lattice* of  $\{1, \dots, N\}$ , defined by set inclusion. We just have to identify complementary pairs  $J, J^c$ , and direct the remaining edges downward, towards smaller slim representatives  $J^c$ . For odd  $N$ , we just attach the artificial vertex  $\mathbf{0}$  on top. For even  $N$ , the artificial vertex replaces the row of half-size pairs  $|J| = |J^c| = N/2$ . This proves (2.22).

As an immediate consequence of the 3-cluster heteroclinic left/right alternatives (b), (c) of (2.3) and (2.4) in theorem 2.2, corollary 2.3, and figure 2.1, the concatenations  $\Theta_*(t)$  of corollary 2.6 can be composed from an arbitrary sequence of left/right rebellions by single rebels  $N_2 = |J_2| = 1$ . See figures 2.2–2.3.

**2.8 Corollary** (Finite 2-shift of heteroclinic concatenations). *For  $n \geq 1$ , let  $\Theta_{\pm}$  denote any two 1- or 2-cluster equilibria with sizes  $N_+ = N_- + n$  and order parameters  $0 < R_- < R_+ \leq 1$ . Prescribe any finite sequence*

$$(2.23) \quad s = s_1 s_2 \dots s_n$$

*of  $n$  sign symbols  $s_{\ell} \in \{\pm\}$ . Consider any associated cascading sequence (2.16) of heteroclinic orbits  $\vartheta_1(t), \dots, \vartheta_n(t)$  between equilibria  $\Theta_- = \Theta_0, \dots, \Theta_n = \Theta_+$  with fat clusters of sizes  $N_- + \ell$ . Each heteroclinic  $\vartheta_{\ell}(t)$  increases the size of the fat cluster by 1, and hence is an isolated one-man rebellion with size  $N_2 = 1$  of the rebellious cluster  $J_2$ . In particular, each  $\vartheta_{\ell}(t)$  is a 3-cluster orbit. Each  $\vartheta_{\ell}(t)$  can be chosen of left or right type (b) or (c), as prescribed by symbol  $s_{\ell} = -$  or  $s_{\ell} = +$ , respectively; see (2.5) and corollary 2.3.*



Corollary 2.6 then provides a total of  $2^n$  distinct transverse concatenations  $\Theta_*(t)$ , one for each left/right sign sequence  $s$ . The concatenations are not related by any permutation or phase-shift symmetry in  $G = S_N \times \mathbb{S}^1$ . Locally, each concatenation generates an  $(n-1)$ -dimensional family of heteroclinic orbits from  $\Theta_-$  to  $\Theta_+$ . According to (2.6), the positions  $x_1 = \vartheta_j$  in the initial fat cluster  $J_0$  shift by a cumulative total

$$(2.24) \quad x_+ - x_- = \frac{\pi}{N} \sum_{\ell=1}^n s_\ell 1.$$

For  $n \geq 2$ , the concatenations  $\Theta_*(t)$  are not realizable by direct 3-cluster heteroclinic orbits, which would require cluster size  $N_2 = n$ . Reflection  $\vartheta \mapsto -\vartheta$ , as in (1.7), swaps cases (b), (c) of figure 2.1. Upon concatenations (2.23), however, the swap affects all symbols  $s_\ell$ , in parallel. This reduces the total count  $2^n$  of corollary 2.8 to  $2^{n-1}$ , but does not affect the exponential growth of available shift-sequences  $s$ , with  $n$ .

Of course we may formulate variants which involve  $n' < n$  symbols  $s_\ell$  and concatenate 3-cluster rebellions which also admit larger rebellious left/right clusters  $J_{\ell,2}$  of general sizes  $N_{2,1} + \dots + N_{2,n'} = n$ . This provides a total count of  $2 \cdot 3^{n-1}$  heteroclinic concatenations  $\Theta_*(t)$ :  $\Theta_0 \rightsquigarrow \Theta_n$  which are not related by any permutation or phase-shift symmetry. Based on the following theorem 2.9, we may also split each rebel cluster set  $J_{\ell,2}$  further, into swarms of subclusters, left/right subclusters, and their concatenations, as sizes permit.

Indeed, the general heteroclinic orbit  $\vartheta_*(t)$ :  $\Theta_- \rightsquigarrow \Theta_+$  is neither a 3-cluster, nor a concatenation of one-man rebellions. For any index set  $J$ , let the subgroup  $S_J \leq S_N$  denote the permutations on  $J$ , i.e. those permutations which fix all elements of the complement  $J^c$ . Let  $\text{Fix}(S_J)$  denote the elements  $\vartheta \in \Xi$  which are fixed under all elements of  $S_J$ . In other words,  $\text{Fix}(S_J)$  collects those  $\vartheta$  which possess a cluster containing  $J$ . The following theorem refines theorem 2.1 and describes the *swarming behavior* of general rebellions. See figure 2.5 for illustration.

**2.9 Theorem** (Realization of arbitrary heteroclinic partitions). *Let  $\vartheta_*(t)$ :  $\Theta_- \rightsquigarrow \Theta_+$  denote any heteroclinic orbit of the Kuramoto model (1.2) between two equilibria  $\Theta_\pm$  with order parameters  $0 < R_- < R_+ < 1$  and fat cluster sets  $J_\pm$ , respectively. Then  $\vartheta_*(t)$  possesses  $M \geq 3$  clusters. More precisely,*

$$(2.25) \quad \vartheta_*(t) \in \text{Fix}(S_{J_-}) \cap \text{Fix}(S_{J_+^c})$$

*inherits the fat cluster set  $J_1 := J_-$  of the source  $\Theta_-$  and the slim cluster set  $J_M := J_+^c$  of the target  $\Theta_+$ , of sizes  $N_-$  and  $N - N_+$ , respectively. Their complementary rebel set  $\hat{J} := J_2 \cup \dots \cup J_{M-1}$  of size  $N_+ - N_- \geq 1$  collects the remaining  $1 \leq M - 2 \leq N_+ - N_-$  clusters.*

*Let the locations  $x_1 < x_m < x_1 + 2\pi$  of these remaining clusters  $1 < m < M$  be ordered by  $m$  without loss of generality. Then they are separated by some  $m_*$  to fall into the left interval  $x_M < x_m < x_1 + 2\pi$ , for  $m_* < m < M$ , and into the right interval  $x_1 < x_m < x_M$ , for  $1 < m \leq m_*$ . See (2.3), (2.4), and figure 2.1. Conversely, each such clustering and separation is realized by certain (families of) heteroclinic orbits  $\vartheta_*(t)$ .*

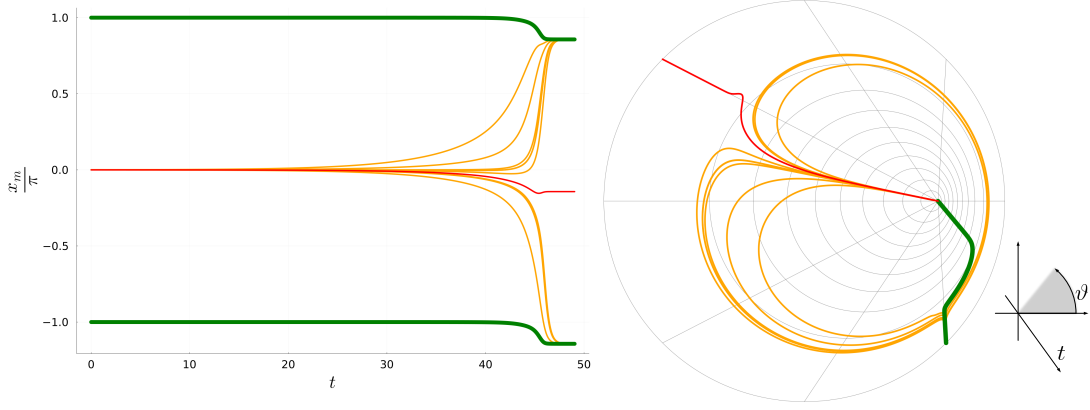


**Figure 2.5:** Time plot of a swarming rebellion from a 2-cluster equilibrium  $\Theta_-$  at  $t \rightarrow -\infty$  towards a 2-cluster equilibrium  $\Theta_+$  with larger fat cluster size. See theorem 2.9. The color coding is the same as in figures 2.2–2.3. Cluster sizes are  $N_- = 11$ ,  $N_+ = 20$  for  $N = 21$  oscillators  $\vartheta_*(t)$ , moving in  $M = 11$  clusters. Limiting cluster phases  $x_1/\pi = -10/21$  and  $x_2/\pi = \dots = x_{11}/\pi = 11/21$  for  $t \rightarrow -\infty$  indicate the same source equilibrium  $\Theta_-$  as in figures 2.2–2.3. Of the  $M = 11$  clusters,  $M - 2 = 9$  are a rebellious swarm of one-man “clusters”, preserving the ordering by phases. The swarm of nine is parted into  $m_* = 5$  right and  $9 - m_* = 4$  left rebels. The final phases at target  $\Theta_+$  satisfy  $x_1/\pi = -11/21$  and  $x_{11}/\pi = 10/21$ .

In figure 2.5 we have chosen initial data  $\vartheta_*(0) \in \text{Fix}(S_{J_-}) \cap \text{Fix}(S_{J_+^c})$  near  $\Theta_+$ . Picking suitable perturbations supported on the swarm indices  $\hat{J}$ , the numerical solution converges to a source 2-cluster equilibrium  $\Theta_-$  in backwards time; see figure 2.5. See section 7 for further comments on the precise choice (7.8) of perturbations, the assignment of left and right rebels by  $m_*$ , and details of numerical implementation.

### 3 Partitioned Coordinates

In this section we set up some notation to prove proposition 1.1 and theorems 2.1(iii)–2.9. Generally speaking, consider the linear orthogonal action  $(\sigma\vartheta)_{\sigma(j)} := \vartheta_j$  of  $\sigma \in S_N$  on the covering space  $\vartheta \in \mathbf{X} = \mathbb{R}^N$  of  $\mathbb{T}^N$ . The orthogonal decomposition into irreducible representations of  $S_N$  is

$$(3.1) \quad \vartheta = x\mathbf{1} \oplus \xi \in \mathbf{X} = \text{span}\{\mathbf{1}\} \oplus \Xi.$$

Here  $\mathbf{1}_j := 1$ , the average of  $\vartheta$  is  $x$ , and  $\xi$  possesses zero average. Note  $\text{span}\{\mathbf{1}\}$  is the space  $\text{Fix}(S_N)$  of  $S_N$ -fixed vectors in  $\mathbf{X}$ . The representation of  $S_N$  on the orthogonal complement  $\Xi = \mathbf{1}^\perp$  is called the *standard irreducible representation* of  $S_N$ . This representation is known to be *absolutely irreducible*, i.e. the only  $S_N$ -equivariant matrices on  $\Xi$  are *real* multiples of the identity matrix. See for example [Elm01, StElCo03, Elm04]. In other words, Schur’s Lemma holds over  $\mathbb{R}$  rather than just over  $\mathbb{C}$ . The angle normalization (1.11), for example, leads to  $x = 0$  in our coordinates, so that  $\xi \in \Xi \cong \mathbb{R}^{N-1}$  measures the deviation from total synchrony.

Next, we extend the above notation to arbitrary partitions (1.8) of the  $N$ -oscillator index set into disjoint subsets  $J_m$  for  $m = 1, \dots, M$ . The index partition induces the following

orthogonal direct sum decomposition of  $\mathbf{X} = \mathbb{R}^N$  :

$$(3.2) \quad \mathbf{X} = \mathbf{X}_1 \oplus \dots \oplus \mathbf{X}_M,$$

$$(3.3) \quad \mathbf{X}_m = \text{span}\{\mathbf{1}_m\} \oplus \Xi_m,$$

where the components of  $\mathbf{x}_m \in \mathbf{X}_m$  are zero outside  $J_m$ , and hence are only supported on  $J_m$ . Analogously to (3.1) we have decomposed here

$$(3.4) \quad \mathbf{x}_m = x_m \mathbf{1}_m \oplus \xi_m \in \mathbf{X}_m = \text{span}\{\mathbf{1}_m\} \oplus \Xi_m,$$

orthogonally. The components  $\mathbf{1}_{mj}$  are 1 for  $j \in J_m$ , and 0 otherwise. The averages of  $\mathbf{x}_m$  are therefore the scalar coordinates  $x_m$ , and each  $\xi_m$  averages to zero. In particular, we may rearrange the coordinates (3.2)–(3.4) to represent  $\boldsymbol{\vartheta}$  by the  $M$ -partitioned coordinates

$$(3.5) \quad (x_2, \dots, x_M, \xi_1, \dots, \xi_M),$$

with the normalization  $x_1 := -\alpha_1^{-1} \sum_{m \geq 2} \alpha_m x_m$  of (1.11). For example, the normalized  $M$ -clusters with coordinates (1.9) correspond to the case where all  $\xi_m$  vanish.

As in (1.8)–(1.9), let  $\sigma_m \in S_{J_m} \leq S_N$  denote the subgroup of permutations  $\sigma_m$  which only permute indices  $j \in J_m$ , leaving all other indices fixed. The decomposition (3.4) is the orthogonal decomposition of  $\mathbf{X}_m$  into irreducible representations of  $S_{J_m}$ . Similarly, the decompositions (3.2)–(3.4) provide the orthogonal decomposition of  $\mathbf{X}_m$  into irreducible representations of the direct product  $S_{\mathbf{J}}$  of all  $S_{J_m}$  for  $m = 1, \dots, M$ . Note that all summands  $\Xi_m$  are pairwise inequivalent, absolutely irreducible representations of  $S_{\mathbf{J}}$ . The span of all  $\mathbf{1}_m$  features the trivial representation of  $S_{\mathbf{J}}$ .

Let  $S'_{J_m}$  denote the direct product of all  $S_{J_{m'}}$  with  $m' \neq m$ . Similarly, let  $\mathbf{X}'_m$  and  $\Xi'_m$  denote the direct sums of all  $\mathbf{X}_{m'}$  and  $\Xi_{m'}$  with  $m' \neq m$ , respectively. Then

$$(3.6) \quad \begin{aligned} \text{Fix}(S_{J_m}) &= \text{Fix}(S_{\mathbf{J}}) \oplus \Xi'_m, \\ \text{Fix}(S'_{J_m}) &= \text{Fix}(S_{\mathbf{J}}) \oplus \Xi_m, \end{aligned}$$

where  $\text{Fix}(S_{\mathbf{J}}) = \text{span}\{\mathbf{1}_m \mid 1 \leq m \leq M\}$  in  $M$ -partitioned coordinates (3.5). By  $S_N$ -equivariance, any such fix space is a time-invariant subspace of the normalized Kuramoto model (1.2).

As the first example, the proof of proposition 1.1 is based on linearizations at 1- and 2-cluster equilibria  $\Theta_{\pm}$  in 2-partitioned coordinates  $(x_2, \xi_1, \xi_2)$ .

**Proof of proposition 1.1.** We start with the linearization  $A := \mathbf{f}'(\Theta)$  at the unique 1-cluster equilibrium  $\Theta = 0$  under the phase constraint (1.11). Note that  $A$  commutes with the isotropy of  $\Theta = 0$ , i.e. with the full permutation group  $S_N$ . Since  $S_N$  acts absolutely irreducibly on  $\mathbf{X} = \Xi$ , the matrix  $A = a \text{Id}$  is a real scalar multiple of identity, and hence

$$(3.7) \quad a = \partial_{\vartheta_j} f_j(0) = -\frac{1}{N} \sum_{k=1}^N \cos(\Theta_k - \Theta_j) = -1,$$

for any  $j$ . This proves claim (i) of proposition 1.1.

We address proposition 1.1(ii) next, and consider the linearization  $A = \mathbf{f}'(\Theta)$  in  $\mathbf{X}$  at any 2-cluster equilibrium  $\Theta$  with  $0 < R = 2\alpha - 1 < 1$ . Let  $J_1$  and  $J_2 = J_1^c$  indicate the partition  $\mathbf{J}$  into fat and slim cluster set, respectively. Then  $M = 2$  and we can invoke 2-partitioned coordinates  $(x_2, \xi_1, \xi_2)$  for  $\vartheta$ ; see (3.5). Since the absolutely irreducible representations of  $S_{\mathbf{J}} = S_{J_1} \times S_{J_2}$  on  $x_2 \in \mathbb{R}$  and the components  $\Xi_1, \Xi_2$  are inequivalent, we can rewrite the linearization  $A$  in block diagonal form with respect to these coordinates:

$$(3.8) \quad A = \begin{pmatrix} a_0 & 0 & 0 \\ 0 & a_1 & 0 \\ 0 & 0 & a_2 \end{pmatrix}.$$

Here  $a_0 \in \mathbb{R}$ , and  $a_1, a_2$  are real scalar multiples of the (omitted) identity matrices  $\text{Id}_m$  on  $\Xi_m$ .

For the linearization  $a_0$  within the 2-cluster subspace of vanishing  $\xi_1, \xi_2$ , the 2-cluster dynamics (1.10) and the phase constraint (1.11) for  $M = 2$  imply

$$(3.9) \quad a_0 = +1.$$

Compare also our discussion of normalized 2-cluster dynamics in (1.12)–(1.13).

To determine  $a_m$  for  $m = 1, 2$ , we fix  $\xi \in \Xi_m$  with  $\xi_j = 1$  for some  $j \in J_m$ . Then the block diagonal structure of  $A$  implies

$$(3.10) \quad \begin{aligned} a_m &= f'_j(\vartheta)\xi = \frac{1}{N} \sum_{k=1}^N \cos(\Theta_k - \Theta_j)(\xi_k - \xi_j) = -(\alpha_m - (1 - \alpha_m)) \\ &= \begin{cases} -2\alpha + 1 = -R < 0, & \text{for } m = 1, \\ +2\alpha - 1 = +R > 0, & \text{for } m = 2. \end{cases} \end{aligned}$$

Here we have used  $\sum \xi_k = 0$ ,  $x_{m'} - x_m = \pm\pi$  for  $m' \neq m$ , and  $\alpha = \alpha_1 = 1 - \alpha_2$ .

Together, (3.9) and (3.10) collect a Morse index

$$(3.11) \quad i(\Theta) = 1 + \dim(\Xi_2) = 1 + (N_2 - 1) = N_2,$$

because  $\Xi_2$  consists of zero-sum vectors whose entries in  $J_2^c$  are zero. This proves claim (ii) of proposition 1.1.

Instability claim (iii) for the algebraic variety  $\{\Theta \in \Xi \mid R = 0\}$  of  $N$ -bar linkage equilibria follows from the fact that  $R \geq 0$  is a strictly increasing Lyapunov function, locally, as soon as  $R > 0$ . This completes the proof of proposition 1.1.  $\bowtie$

## 4 Stable and unstable manifolds

We can now describe the stable and unstable manifolds of hyperbolic 2-cluster equilibria  $\Theta$  with order parameter  $0 < R = 2\alpha - 1 < 1$ ; see lemma 4.1. In lemma 4.2, we collect some consequences for general heteroclinic orbits  $\vartheta_*(t)$ :  $\Theta_- \rightsquigarrow \Theta_+$  between 2-cluster equilibria  $\Theta_{\pm}$ . In particular, lemma 4.2 proves monotonicity of fat clusters, i.e. theorem 2.1(iii). Our presentation relies on proposition 1.1 and partitioned coordinates (3.5) in the  $\mathbb{S}^1$ -section (1.11).

**4.1 Lemma** (Invariant manifolds are fixed). *Let  $\Theta$  be any equilibrium of the Kuramoto model (1.2) with order parameter  $0 < R = 2\alpha - 1 < 1$ . Let  $J = J_1$  and  $J^c = J_2$  denote the fat and slim clusters of  $\Theta$  with size fractions  $1/2 < \alpha < 1$  and  $\alpha_c = 1 - \alpha$ , respectively. In the  $M = 2$  partitioned coordinates  $(x_2, \xi_1, \xi_2)$  of (3.5), the stable and unstable manifolds  $W^{s,u}$  of  $\Theta$  then possess the tangent spaces*

$$(4.1) \quad T_{\Theta}W^u = \text{Fix}(S_{J_1}) = \mathbf{X}'_1 = \mathbf{X}_2 = \text{span}\{\mathbf{1}_2\} \oplus \Xi_2,$$

$$(4.2) \quad T_{\Theta}W^s = \text{Fix}(S_{J_2}) \cap \{x_2 = 0\} = \Xi_1,$$

$$(4.3) \quad T_{\Theta}W^s \leq \text{Fix}(S_{J_2}) = \text{span}\{\mathbf{1}_2\} \oplus \Xi_1,$$

at any  $\vartheta$ . Since the linear spaces  $\text{Fix}(S_{J_m})$  are time-invariant, this implies

$$(4.4) \quad W^u \subseteq \text{Fix}(S_{J_1}) = \text{span}\{\mathbf{1}_2\} \oplus \Xi_2,$$

$$(4.5) \quad W^s \subsetneq \text{Fix}(S_{J_2}) = \text{span}\{\mathbf{1}_2\} \oplus \Xi_1.$$

Both  $T_{\vartheta}W^s$  and  $W^s$  are of codimension 1 in  $\text{Fix}(S_{J_2})$ , respectively.

**Proof.** We first establish the linear claim (4.1) at the equilibrium  $\vartheta = \Theta$ . Next, we show how (4.1) at  $\vartheta = \Theta$  implies the nonlinear claim (4.4). Linearization at any  $\vartheta \in W^u$  then implies (4.1) everywhere. We conclude with the very similar arguments for (4.2), (4.3), and (4.5).

By proposition 1.1(ii), the equilibrium  $\Theta$  is a hyperbolic 2-cluster. In (3.9)–(3.10) we have determined the unstable eigenvalues  $a_0 = +1$ , in the 2-partitioned coordinate  $x_2$  of  $\text{span}\{\mathbf{1}_2\}$ , and  $a_2 = R = 2\alpha - 1 > 0$ , in the coordinates  $\xi_2 \in \Xi_2$ . This proves the linear claim (4.1) at  $\vartheta = \Theta$ . The stable eigenvalue  $a_1 = -R < 0$  in the complementary eigenspace  $\Xi_1$  proves (4.3).

To prove the nonlinear claim (4.4), we rely on invariance of the linear space  $\text{Fix}(S_{J_1})$  in (4.1) under the nonlinear flow of (1.2); see (3.6). We therefore obtain a local unstable manifold  $W_{\text{loc}}^u$  of  $\Theta$  within  $\text{Fix}(S_{J_1})$ . In fact,  $W_{\text{loc}}^u$  coincides with that tangent space, locally. Since  $W_{\text{loc}}^u$  and  $W^u$  are unique, this proves claim (4.4). Linearization and invariance of dimension then implies claim (4.1) at any  $\vartheta \in W^u$ .

To prove nonlinear claim (4.5), we first have to confess that nonlinear time-invariance of the representation subspace  $\Xi_1$  may fail. Moreover, the tangent space  $T_{\Theta}W^s$  needs to be attached to  $\Theta \in \text{span}\{\mathbf{1}_2\}$ . Working in the nonlinearly time-invariant linear space  $\text{Fix}(S_{J_2})$ , however, proves claim (4.3) by uniqueness of  $W^s$ . Linearization then implies claim (4.3) and determines the codimensions 1. This proves the lemma.  $\bowtie$

**4.2 Lemma** (Invariant manifolds are linear). *Let  $\vartheta_*(t)$ :  $\Theta_- \rightsquigarrow \Theta_+$  denote any heteroclinic orbit between equilibria  $0 < R(\Theta_-) = 2\alpha_- - 1 < 2\alpha_+ - 1 = R(\Theta_+) < 1$ . Then  $\Theta_{\pm}$  are 2-cluster equilibria, by theorem 2.1(i), with fat clusters of size fractions  $\alpha_{\pm}$  and complementary slim clusters  $J_{\pm}^c$ . Moreover, the fat clusters grow strictly,*

$$(i) \quad \vartheta_* \in \text{Fix}(S_{J_-}) \cap \text{Fix}(S_{J_+^c});$$

$$(ii) \quad \alpha_- < \alpha_+ \text{ and } J_- \subsetneq J_+.$$

Let  $(x_2, x_3, \xi_1, \xi_2, \xi_3)$  denote the 3-partitioned coordinates (3.5) of  $\vartheta_*(t)$  for the resulting index partition  $\mathbf{J}$  of (2.1) given by  $J_1 := J_-$ ,  $J_2 := J_+ \setminus J_-$ ,  $J_3 := J_+^c$ . Then

$$(4.6) \quad \xi_1 = 0 \text{ and } \xi_3 = 0.$$

The tangent spaces  $T_*W_-^u$  and  $T_*W_+^s$  to the stable and unstable manifolds of  $\Theta_\pm$  at any  $\vartheta_* = \vartheta_*(t)$  satisfy

$$(4.7) \quad T_*W_-^u = \text{Fix}(S_{J_1}) = \mathbf{X}_2 \oplus \mathbf{X}_3 = \text{span}\{\mathbf{1}_2, \mathbf{1}_3\} \oplus \Xi_2 \oplus \Xi_3,$$

$$(4.8) \quad T_*W_+^s \leq \text{Fix}(S_{J_3}) = \mathbf{X}_1 \oplus \mathbf{X}_2 \oplus \text{span}\{\mathbf{1}_3\} = \text{span}\{\mathbf{1}_2, \mathbf{1}_3\} \oplus \Xi_1 \oplus \Xi_2.$$

Here  $T_*W_+^s$  is of codimension 1 in  $\text{Fix}(S_{J_3})$ .

In the case  $R(\Theta_+) = 1$  of a totally synchronous 1-cluster target  $\Theta_+ = 0$ , the results hold with  $\alpha_+ = 1$ ,  $J_3 = J_+^c = \emptyset$ . Moreover  $T_*W_+^s = \text{Fix}(S_{J_+^c}) = \Xi$  without codimension.

**Proof.** We prove the claims, in order of appearance. The trivial adaptations to the synchronous 1-cluster case  $\Theta_+ = 0$  will be omitted.

Claim (i) follows from (4.4)–(4.5) in lemma 4.1, applied to  $\Theta = \Theta_\pm$ .

To prove the strong monotonicity claim (ii), we first note  $\alpha_- < \alpha_+$ , by strict increase of the order parameter  $0 < R < 1$  along  $\vartheta_*$ . This mere increase in size already excludes the homoclinic case  $\Theta_+ = \Theta_-$  and the case  $J_+ = J_-$ . It remains to prove the weak monotonicity claim  $J_+ \supseteq J_-$ . We apply (4.4) with  $\Theta = \Theta_-$  to  $W_-^u \ni \vartheta_*(t)$  in the closed time-invariant subspace

$$(4.9) \quad \Theta_+ = \lim_{t \rightarrow \infty} \vartheta_*(t) \in \text{Fix}(S_{J_-}).$$

In particular, the components  $\Theta_{+,j}$  with  $j \in J_-$  all coincide. On the other hand, the 2-cluster equilibrium  $\Theta_+$  has only two values of  $\Theta_{+,j}$  to offer, mod  $2\pi$ : the value  $x_+ = (\alpha_+ - 1)\pi$ , for  $j \in J_+$ , and the value  $x_+^c = \alpha_+\pi$  for complementary  $j \in J_+^c$ . Since both clusters  $J_\pm$  are fat, (4.9) implies weak monotonicity  $J_+ \supseteq J_-$ .

This proves claim (ii) and strong monotonicity of fat clusters, theorem 2.1(iii). It also justifies the  $M = 3$  partition  $\mathbf{J}$  by  $J_1 := J_-$ ,  $J_2 := J_+ \setminus J_-$ ,  $J_3 := J_+^c$ . We proceed via the associated 3-partitioned coordinates  $(x_2, x_3, \xi_1, \xi_2, \xi_3)$ ; see (3.5).

Claim (4.6) follows by definition of the 3-partitioned components  $\xi_1, \xi_3$  associated to  $J_1 = J_-$  and  $J_3 = J_+^c$ . Indeed, (4.4) and (4.5) apply to  $\vartheta_+(t) \in W_-^u \cap W_+^s$  and imply

$$(4.10) \quad \vartheta_*(t) \in \text{Fix}(S_{J_-}) \cap \text{Fix}(S_{J_+^c}).$$

Claims (4.7) and (4.8) follow from (4.1) and (4.3), similarly and respectively, in 3-cluster coordinates  $(x_2, x_3, \xi_1, \xi_2, \xi_3)$ . Here we have used (3.6) to prove the last equality in (4.7). To prove claim (4.8), we have started from (4.3) to proceed in the same way:

$$(4.11) \quad T_*W_+^s \leq \text{Fix}(S_{J_3}) = \text{span}\{\mathbf{1}_2, \mathbf{1}_3\} \oplus \Xi_1 \oplus \Xi_2.$$

Recall how the subspace inclusion  $\leq$  is of codimension 1. This proves the lemma, and theorem 2.1(iii).  $\bowtie$

## 5 Three-cluster orbits

Consider any pair  $\Theta_\pm$  of 2-cluster equilibria with order parameters  $0 < R_- = 2\alpha_- - 1 < 2\alpha_+ - 1 = R_+ < 1$ , fat size fractions  $\alpha_\pm$ , and associated  $M = 3$  index partition  $\mathbf{J}$  given by



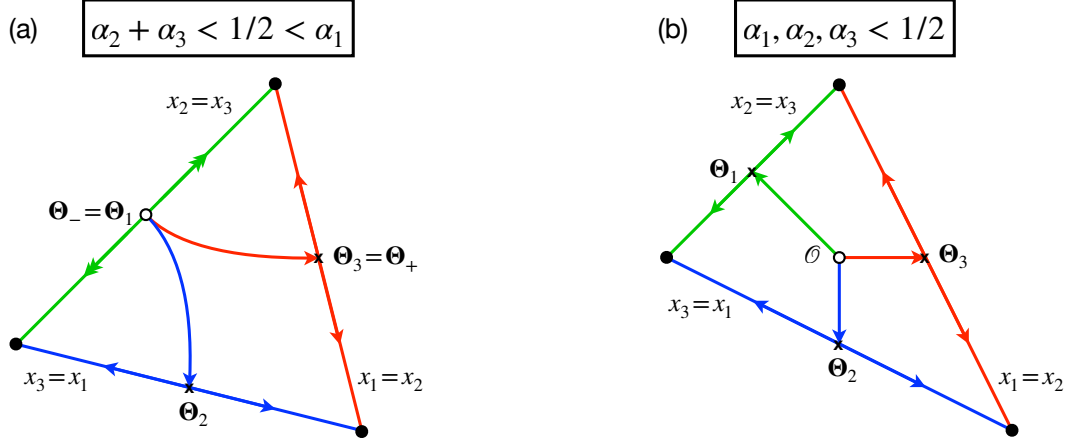


**Figure 5.1:** Qualitative dynamics on fundamental triangles of the 3-cluster flows (5.1) under the phase constraint (1.11), in the coordinate plane  $(x_2, x_3)$ . The vertices  $\Theta = 0$  (solid dots) are torus copies of the 1-cluster equilibrium  $x_1 = x_2 = x_3 = 0$ . The three sides are the time-invariant lines  $x_{m+1} = x_{m+2}$ , with indices  $m \bmod 3$ , along with their torus copies. Each side contains a unique nontrivial 2-cluster equilibrium  $\Theta_m$ , at its midpoint. Compare (1.12)–(1.13) and proposition 1.1.

**Case (a):**  $1/2 < \alpha_1 < 1$ . For illustration, we have used size fractions  $(\alpha_1, \alpha_2, \alpha_3) = (3, 1, 1)/5$ . The 2-cluster equilibrium  $\Theta_- = \Theta_1$  (circle) possesses a fat cluster of size fraction  $1/2 < \alpha_1 = N_1/N < 1$ . It is unstable, with fast unstable eigenvalue  $\mu_1 = +1$  along its side (green) and slow unstable eigenvalue  $0 < \mu_2 = 2\alpha_1 - 1 < 1$  towards the interior. The equilibria  $\Theta_2$  and  $\Theta_3 = \Theta_+$  (cross marks) possess fat clusters of larger size fractions  $\alpha_1 + \alpha_3$  and  $\alpha_+ = \alpha_1 + \alpha_2$ , respectively. They are hyperbolic saddles with  $\mu_2 < 0 < \mu_1 = +1$ . The stable and unstable manifolds are colored blue for  $\Theta_2$ , and red for  $\Theta_3$ .

**Case (b):**  $0 < \alpha_1, \alpha_2, \alpha_3 < 1/2$ . For illustration, we have used size fractions  $(\alpha_1, \alpha_2, \alpha_3) = (1, 1, 1)/3$ . All three 2-cluster equilibria  $\Theta_m$  are hyperbolic saddles (cross marks), with their sides as unstable manifolds as before. Their time-invariant manifolds are colored green, blue, and red, respectively. The interior of each fundamental triangle features a unique 3-cluster, 3-bar linkage equilibrium  $\mathcal{O}$  (circle) with order parameter  $R = 0$ . The increasing Lyapunov function  $R$  implies total instability of  $\mathcal{O}$ . Hence, the green, red, and blue stable manifolds of the 2-cluster saddles  $\Theta_m$  emanate from the interior 3-cluster equilibrium.

$J_1 := J_-$ ,  $J_2 := J_+ \setminus J_-$ ,  $J_3 := J_+^c$ ; see theorem 2.1(iii) and (2.1). Theorem 2.2 requires the construction of a 3-cluster heteroclinic orbit  $\vartheta_*(t)$ :  $\Theta_- \rightsquigarrow \Theta_+$ . We therefore start from any such 3-cluster partition with size ratios  $0 < \alpha_2, \alpha_3 < 1/2 < \alpha_1 < 1$ . The proof of theorem 2.2 will then follow from a detailed analysis of the flow of arbitrary 3-cluster solutions  $\vartheta(t)$ . In the 3-cluster coordinates  $(x_1, x_2, x_3)$  of (1.10) with  $M = 3$ , we have to discuss

$$(5.1) \quad \dot{x}_m = \alpha_{m-1} \sin(x_{m-1} - x_m) + \alpha_{m+1} \sin(x_{m+1} - x_m),$$

for indices  $m \bmod 3$ . The time-invariant phase constraint (1.11) eliminates uniform phase shifts by  $x_1 := -\alpha_1^{-1}(\alpha_2 x_2 + \alpha_3 x_3)$ . This defines a 2-torus  $\mathbb{T}^2$  in the coordinates  $(x_2, x_3)$  of the constraint space  $\Xi$  of (1.11). Abstractly, the period lattice in the constraint space  $\Xi \cap \text{Fix}(S_J) \cong \mathbb{R}^2$  of normalized cluster coordinates is given by the projection of the lattice  $2\pi\mathbb{Z}^3$  along the vector  $(1, 1, 1)$  of the  $\mathbb{S}^1$ -action (1.5). In other words, the period lattice consists of those normalized  $(x_1, x_2, x_3)$  for which there exists some  $\psi$  such that all  $x_m + \psi \in 2\pi\mathbb{Z}$ . The synchronous 1-cluster equilibrium copies arise as  $x_1 = x_2 = x_3 = 0 \bmod \mathbb{T}^2$  (solid dots in figures 5.1–5.2) and therefore coincide with the period lattice of  $\mathbb{T}^2$ .

Any 2-cluster equilibria  $\Theta_m$  must arise, in this system (5.1), via  $x_{m-1} = x_{m+1}$  distinct

from  $x_m$ , and with indices  $m \bmod 3$ . This leads to the three distinct time-invariant lines  $x_2 = x_3$ ,  $x_3 = x_1$ , and  $x_1 = x_2$ , respectively. Our description (1.12) of 2-cluster dynamics applies to each such line with notation (1.13) adapted to the lines in  $(x_2, x_3) \in \mathbb{T}^2$ . Three lines intersect where any two do, because any such intersection represents a copy of the totally synchronous 1-cluster equilibrium in  $\mathbb{T}^2$ . From (1.12)–(1.13) and proposition 1.1 we recall that the nontrivial 2-cluster equilibria  $\Theta_m$  are located at the midpoints of each side of the resulting *fundamental triangles*.

In variables  $(x_2, x_3)$ , figure 5.1(a) sketches the case where one cluster is fat and the other two clusters remain slim, even when combined, i.e.

$$(5.2) \quad 0 < \alpha_2 + \alpha_3 < 1/2 < \alpha_1 < 1.$$

The only 3-cluster equilibria, which are not degenerate 2- or 1-clusters in disguise, arise as distinct 3-bar linkages with  $R = 0$  in the alternative case

$$(5.3) \quad 0 = \alpha_1 \exp(ix_1) + \alpha_2 \exp(ix_2) + \alpha_3 \exp(ix_3);$$

see (1.14). Such triangles with distinct angles  $x_1, x_2, x_3$  arise if, and only if

$$(5.4) \quad 0 < \alpha_1, \alpha_2, \alpha_3 < 1/2.$$

Indeed all other cases lead to linearly degenerate triangles, or violate the triangle inequality. In figure 5.1(b) we sketch (5.4), again in variables  $(x_2, x_3)$ .

We study case (5.4) first. We linearize (5.1) at the 2-cluster equilibrium  $\Theta_1$  defined by  $x_2 = x_3 = x_1 + \pi$ . In coordinates  $(y_1, y_2, y_3)$  which underlie the same phase constraint (1.11) we obtain

$$(5.5) \quad \begin{aligned} \dot{y}_1 &= -\alpha_2(y_2 - y_1) - \alpha_3(y_3 - y_1), \\ \dot{y}_2 &= +\alpha_3(y_3 - y_2) - \alpha_1(y_1 - y_2), \\ \dot{y}_3 &= -\alpha_1(y_1 - y_3) + \alpha_2(y_2 - y_3). \end{aligned}$$

The linearization possesses an eigenvalue  $\mu_1 = +1$  along the time-invariant 2-cluster line  $y_2 = y_3$ , because the constraint (1.11) then implies  $\alpha_1 y_1 + (1 - \alpha_1)y_2 = \alpha_1 y_1 + (1 - \alpha_1)y_3 = 0$ . This agrees with (3.9). Since the constraint (1.11) contributes a zero eigenvalue to the linearization of (5.1), the other nontrivial eigenvalue  $\mu_2$  is related to the trace of the right hand side of (5.5) by

$$(5.6) \quad \mu_2 = \text{trace} - \mu_1 = (\alpha_2 + \alpha_3) + (-\alpha_3 + \alpha_1) + (\alpha_1 - \alpha_2) - 1 = 2\alpha_1 - 1.$$

By cyclic permutations of indices, or by (3.8), this proves  $\mu_1 = +1$  within their invariant line, at all 2-clusters, and

$$(5.7) \quad \mu_2 = \begin{cases} 2\alpha_1 - 1, & \text{at } x_2 = x_3; \\ 2\alpha_2 - 1, & \text{at } x_3 = x_1; \\ 2\alpha_3 - 1, & \text{at } x_1 = x_2. \end{cases}$$

In the 3-bar linkage triangle case (5.4) this implies a stable eigenvalue  $\mu_2 < 0$  towards the interior, of all boundary saddles; see figure 5.1(b) The interior rational 3-bar linkage chain equilibrium  $\mathcal{O}$  is totally unstable.



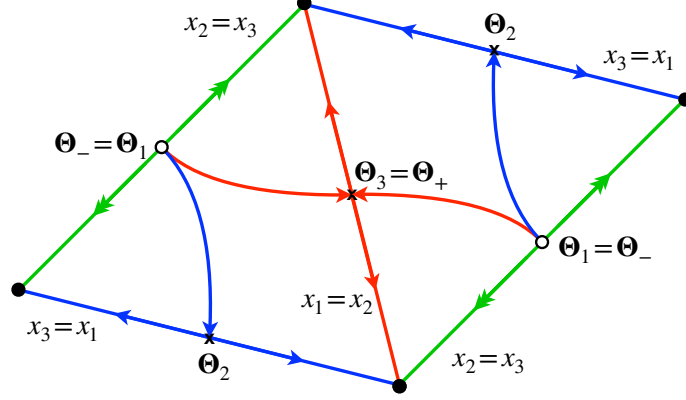


**Figure 5.2:** We consider the fat/slim case of figure 5.1(a), in the same notation and colors. The fundamental parallelogram of the 3-cluster dynamics consists of two adjacent copies of the fundamental triangle of figure 5.1(a). The two branches  $\vartheta_*(t)$  of the stable manifold (red) arrive at their target equilibrium  $\Theta_+ = \Theta_3$  along the same horizontal tangent, but from opposite sides  $x_2$ . In theorem 2.2, this generates the two options (2.3), (2.4) for 3-cluster heteroclinic orbits  $\vartheta_*(t)$ :  $\Theta_- \rightsquigarrow \Theta_+$ .

In the opposite case  $\alpha_1 > 1/2 > \alpha_2 + \alpha_3$  of figure 5.1(a), we see that only the boundary 2-cluster equilibrium  $\Theta_1$  at  $x_2 = x_3$  is two-dimensionally unstable. The other two boundary 2-cluster equilibria  $\Theta_2$  and  $\Theta_3$  remain hyperbolic saddles, as before. For  $0 < \mu_2 = 2\alpha_1 - 1 < 1$ , the 2-cluster side  $x_2 = x_3$  of  $\Theta_1$  constitutes the fast unstable manifold. All other unstable orbits emanate from the stationary 2-cluster tangentially to the eigenvector of the slower unstable  $\mu_2$ , as part of its “mustache” [Arn88]. We have omitted the case  $\alpha_1 = 1/2 = \alpha_2 + \alpha_3$  here, because it generates a degenerate 2-cluster equilibrium satisfying  $R = 0$  with a zero eigenvalue  $\mu_2 = 0$  at the boundary  $x_2 = x_3$ . In summary, this establishes the flows of figure 5.1 in the fundamental triangles of the 3-cluster flow on the constrained 2-torus  $\mathbb{T}^2$ .

**Proof of theorem 2.2.** Given any two equilibria  $\Theta_{\pm}$  with order parameters  $0 < R_- < R_+ \leq 1$ , we have to construct a 3-cluster heteroclinic orbit  $\vartheta_*(t)$ :  $\Theta_- \rightsquigarrow \Theta_+$  between them. By theorem 2.1, the source  $\Theta_-$  and the target  $\Theta_+$  are 2-cluster equilibria with fat clusters on  $J_+ \supsetneq J_-$  and complementary slim clusters on  $J_+^c \subsetneq J_-^c$ . Therefore, (2.1) uniquely determines the  $M = 3$  index partition  $J_1 := J_-$ ,  $J_2 := J_+ \setminus J_-$ ,  $J_3 := J_+^c$  of our 3-cluster candidate  $\vartheta_*(t)$ ; see theorem 2.1. This also determines the respective size fractions  $\alpha_1 = \alpha_-$ ,  $\alpha_2 = \alpha_+ - \alpha_-$ ,  $\alpha_3 = 1 - \alpha_+$ . In particular, our assumption  $1/2 < \alpha_{\pm} = (R_{\pm} + 1)/2 < 1$  implies  $1/2 < \alpha_1 = \alpha_- < 1$ .

Our analysis of the 3-cluster flow (5.1) therefore leads to a 3-cluster heteroclinic orbit  $\vartheta_*(t)$ :  $\Theta_1 \rightsquigarrow \Theta_3$ . Moreover, our choice of  $J_1, J_2, J_3$  implies  $\Theta_1 = \Theta_-$  and  $\Theta_3 = \Theta_+$ . Indeed, the fat clusters  $J_1 = J_-$  at  $\Theta_1$  and  $\Theta_-$  coincide, as do the slim clusters  $J_3 = J_+^c$  at  $\Theta_3$  and  $\Theta_+$ , along with their respective complements. This proves that the 3-cluster  $\vartheta_*(t)$ :  $\Theta_- \rightsquigarrow \Theta_+$  is heteroclinic between the prescribed source and target equilibria  $\Theta_{\pm}$ . Claim (2.2) follows by construction of  $J_2$  and the cluster angle relation of theorem 2.1(ii) for the locations  $x_{\pm}$  of the fat clusters, to which the slim clusters are antipodal.

It remains to realize both directional claims (2.3) and (2.4) for suitable instantiations of the 3-cluster heteroclinic orbit  $\vartheta_*(t)$ . This is illustrated in figure 5.2, where we have redrawn two oppositely oriented copies of the fundamental triangle of figure 5.1(a). The

two copies, together, define a *fundamental parallelogram* of the 2-torus  $\mathbb{T}^2$  which results from our representation of 3-cluster coordinates  $(x_1, x_2, x_3)$  by  $(x_2, x_3)$ , under the phase constraint (1.11). We see the two branches of the stable manifold arriving at their target equilibrium  $\Theta_+ = \Theta_3$  along the same horizontal tangent, but from opposite sides  $x_2$ . Compare (4.2). Likewise, the two branches emanate from the unstable source equilibrium  $\Theta_- = \Theta_1$  along the same slow unstable eigenvector tangent  $0 < \mu_2 = 2\alpha_1 - 1 < +1 = \mu_1$ , perpendicularly to the invariant fast unstable boundary of eigenvalue  $\mu_1$ , but in opposite directions. This distinguishes, and realizes, both options (2.3) and (2.4) for 3-cluster heteroclinic orbits  $\vartheta_*(t)$ :  $\Theta_- \rightsquigarrow \Theta_+$ .

The remaining 2-cluster heteroclinic orbit  $\Theta_1 = \Theta_- \rightsquigarrow \Theta_+ = 0$  towards total synchrony follows from invariance of the boundary line  $x_2 = x_3$ . This completes the proof of theorem 2.2.  $\boxtimes$

## 6 Transversality

Let  $\vartheta_*(t)$ :  $\Theta_- \rightsquigarrow \Theta_+$  denote any heteroclinic orbit between two equilibria  $\Theta_\pm$  with order parameters  $0 < R_- < R_+ < 1$ . By theorem 2.2, we may invoke the 3-partitioned coordinates

$$(6.1) \quad (x_2, x_3, \xi_1, \xi_2, \xi_3) \in \mathbb{R}^2 \oplus \Xi_1 \oplus \Xi_2 \oplus \Xi_3$$

associated to  $\Theta_1 := \Theta_-$  and  $\Theta_3 := \Theta_+$ ; see (3.5). We denote the unstable manifold of  $\Theta_-$  and the stable manifold of  $\Theta_+$  by  $W_-^u$  and  $W_+^s$ , respectively.

**Proof of theorem 2.4.** In case of total synchrony  $\Theta_+ = 0$ ,  $R_+ = 1$ , linear stability of  $\Theta_+$  leaves nothing to be proved.

In the 2-cluster cases  $0 < R_- < R_+ < 1$ , we have to show the left equality of

$$(6.2) \quad T_{\vartheta_*(t)}W_-^u + T_{\vartheta_*(t)}W_+^s = \Xi = \mathbb{R}^2 \oplus \Xi_1 \oplus \Xi_2 \oplus \Xi_3;$$

compare (2.12). The claim is invariant under small perturbations of the tangent spaces. Since the stable manifold  $W_+^s$  is  $C^1$ , and  $\vartheta_*(t) \rightarrow \Theta_+$  for  $t \rightarrow \infty$ , we may equivalently show

$$(6.3) \quad T_{\vartheta_*(t)}W_-^u + T_{\Theta_+}W_+^s = \mathbb{R}^2 \oplus \Xi_1 \oplus \Xi_2 \oplus \Xi_3,$$

for some large  $t \gg 1$ .

For any  $t \in \mathbb{R}$ , lemma 4.2 with  $\vartheta := \vartheta_*(t)$  asserts

$$(6.4) \quad T_{\vartheta_*(t)}W_-^u = \text{Fix}(S_{J_1}) = \mathbb{R}^2 \oplus \Xi_2 \oplus \Xi_3;$$

see (4.7). At the 2-cluster target equilibrium  $\Theta_3 = \Theta_+$ , on the other hand, (4.3) of lemma 4.1 asserts  $T_{\Theta_+}W_+^s = \Xi_1 \oplus \Xi_2$ , in the present 3-partitioned notation. Combined, this proves transversality claim (6.3), and theorem 2.4.  $\boxtimes$

**Proof of theorem 2.9.** We can write any heteroclinic orbit  $\vartheta_*(t)$ :  $\Theta_- \rightsquigarrow \Theta_+$  as an  $M$ -cluster orbit with coordinates  $x_m$ ; see (1.8)–(1.10). Since  $x_m = x_{m'}$  implies  $\dot{x}_m = \dot{x}_{m'}$ ,

we may choose  $M$  minimal so that all  $x_m$  are, and remain, distinct for all times. By theorem 2.1, we have fat equilibrium cluster sets  $J_1 := J_- \subsetneq J_+$  and slim  $J_M = J_+^c$ .

Note  $M \geq 3$  because we have excluded synchronous targets  $\Theta_+ = 0$ ,  $R_+ = 1$ . Moreover  $M - 2 \leq \#(J_+ \setminus J_-) = N_+ - N_-$ , because each of the  $M - 2$  remaining clusters contains at least one element.

Lemma 4.2(i) implies claim (2.25) of the theorem.

Let  $\widehat{J} := J_2 \dot{\cup} \dots \dot{\cup} J_{M-1}$  collect the rebel clusters of  $\vartheta_*(t)$  with ordered coordinates

$$(6.5) \quad x_1 < x_2 < \dots < x_{m_*} < x_M < x_{m_*+1} < \dots < x_{M-1} < x_1 + 2\pi.$$

The ordering, we recall, is time-invariant. The “converse” claim of the theorem requires the construction of heteroclinic orbits  $\vartheta_*(t)$ :  $\Theta_- \rightsquigarrow \Theta_+$  with such an order of the cluster coordinates, for any  $M \geq 3$  and any prescribes  $1 \leq m_* < M$ . For  $M = 3$ , the 3-cluster theorem 2.2 proves just that: see (2.3) for  $m_* = 1$ , and (2.4) for  $m_* = 2$ .

To address  $M \geq 4$ , we invoke lemma 4.2 with  $M$ -partitioned coordinates  $(\widehat{x}, x_M, \xi_1, \widehat{\xi}, \xi_M)$  associated to the index partition  $J_1 \dot{\cup} \widehat{J} \dot{\cup} J_M$  and  $J_1 = J_-$ ,  $J_M = J_+^c$ . By transversality theorem 2.4, the tangent space to the heteroclinic set of  $\vartheta(t)$ :  $\Theta_- \rightsquigarrow \Theta_+$  at any  $\vartheta_*(t)$  is given by

$$(6.6) \quad T_*W_-^u \cap T_*W_+^s \leq \text{Fix}(S_{J_-}) \cap \text{Fix}(S_{J_+^c}) = \text{span}\{\widehat{\mathbf{1}}, \mathbf{1}_{c+}\} \oplus \widehat{\Xi}.$$

Here  $\widehat{\mathbf{1}}$ ,  $\widehat{\Xi}$  refer to  $\widehat{J}$ , and  $\mathbf{1}_{c+}$  refers to  $J_+^c$ . For  $t \rightarrow +\infty$ , more precisely, (4.11) implies

$$(6.7) \quad T_*W_-^u \cap T_*W_+^s \approx \text{span}\{\widehat{\mathbf{1}}\} \oplus \widehat{\Xi},$$

up to an arbitrarily small perturbation in the direction of  $\mathbf{1}_{c+}$ . This allows for any perturbation

$$(6.8) \quad \widetilde{\vartheta}(t) = \Theta_+ + \varepsilon \widehat{\vartheta}(t) + o(\varepsilon)$$

with  $\widehat{\vartheta}(t)$  supported on  $\widehat{J}$ . The components  $\Theta_{+j}$  of the 2-cluster equilibrium  $\Theta_+$  are constant for  $j \in J_+$  and  $j \in J_+^c$ , respectively. Choosing  $\widehat{\vartheta}(t)$  with support on  $\widehat{J}$ , we can therefore realize any prescribed clustering and ordering (6.5) for  $\widehat{\vartheta}(t)$ , and hence for  $\widetilde{\vartheta}(t)$ . Since the orbit of  $\widetilde{\vartheta}(t)$ :  $\Theta_- \rightsquigarrow \Theta_+$  is heteroclinic, by construction (6.8), this proves theorem 2.9.  $\bowtie$

## 7 Numerical solutions

In this section we comment on, and illustrate, concatenations of transverse heteroclinic rebellions among 2-clusters and towards the 1-cluster of total synchrony. See concatenation corollaries 2.6, 2.8 and figures 2.1–2.3, for successive one-man rebellions. For general swarm rebellions, see theorem 2.9 and figure 2.5.

We address one-man rebellions first. These are special cases  $0 < \alpha_3 < 1/2 < \alpha_1 < 1$ ,  $\alpha_2 = 1/N$  of the 3-cluster rebellions studies in theorem 2.2 and section 5.

Prior to their concatenation, we illustrate how to determine heteroclinic saddle-saddle connections. The numerical literature has established numerical methods and codes for such pursuits; see for example [Beyn90, DGK03, KOD05]. The analysis in the 3-cluster phase plane of figure 5.2, however, offers a much more elementary (and cheaper) approach. Indeed, the concatenation corollaries 2.6, 2.8 allow us to approximate each 3-cluster step  $\Theta_- \rightsquigarrow \Theta_+$  in the heteroclinic cascade (2.23), separately. Moreover, total instability of  $\Theta_-$  within the 3-cluster plane of figure 5.2 suggests to trace trajectories *backwards in time*.

Specifically, we start from a phase perturbation denoted by  $\varepsilon = (\varepsilon_1, \varepsilon_2, 0) \in \mathbb{R}^3$  of  $\Theta_+$  such that  $\varepsilon_2 = -s_\ell 10^{-2}$ , where  $s_\ell \in \{-, +\}$  denote the shift symbols in corollary 2.8 and (2.5). To ensure that the perturbation is horizontally tangent to its stable manifold  $W_+^s$ , we impose

$$(7.1) \quad \alpha_1 \varepsilon_1 + \alpha_2 \varepsilon_2 = 0$$

so that  $\varepsilon_1$  is chosen. In particular, the 3-cluster solution of (5.1) which starts from

$$(7.2) \quad \Theta_+ + \varepsilon,$$

in reverse time, obeys the same invariant phase normalization (1.11) as the targeted 2-cluster equilibrium  $\Theta_+$ . Next, we perform the following loop while  $\alpha_1$  remain larger than  $1/2$ .

**Step 1:** Solve the 3-cluster system (5.1) numerically *in backward time* until reaching a stopping time  $t = T$  such that  $x_2(T) - x_3(T) \bmod 2\pi$  is smaller than  $10^{-2}$ . By our rigorous analysis of the dynamics on the fundamental triangles in figure 5.1, we conclude that  $0 > T > -\infty$  is finite and we are numerically close to a copy of the source 2-cluster equilibrium  $\Theta_-$ .

**Step 2:** Note how  $\Theta_-$  coincides with the 2-cluster equilibrium  $\tilde{\Theta}_+$  in the 3-cluster system (5.1) with updated cluster fractions

$$(7.3) \quad (\tilde{\alpha}_1, \tilde{\alpha}_2, \tilde{\alpha}_3) = (\alpha_1 - \alpha_2, \alpha_2, \alpha_3 + \alpha_2).$$

Choose a small perturbation  $\tilde{\varepsilon} = (\tilde{\varepsilon}_1, \tilde{\varepsilon}_2, 0) \in \mathbb{R}^3$  such that  $\tilde{\varepsilon}_2 = -s_\ell 10^{-2}$  and

$$(7.4) \quad \tilde{\alpha}_1 \tilde{\varepsilon}_1 + \tilde{\alpha}_2 \tilde{\varepsilon}_2 = 0.$$

While decreased  $\tilde{\alpha}_1 > 1/2$ , repeat **Step 1** with updated cluster fractions and initial data

$$(7.5) \quad \tilde{\Theta}_+ + \tilde{\varepsilon}.$$

By this procedure, we obtain numerical approximations of the rebellious sequences shown in corollary 2.6, backwards in time. **Step 2** jumps from a backwards solution in  $W_{\text{loc}}^u(\Theta_-)$ , which terminates near  $\Theta_- = \tilde{\Theta}_+$ , to a new initial condition (7.5). We then solve (5.1), with updated size fraction parameters (7.3) and on a different fundamental domain. Of course, this amounts to a jump between 3-cluster solutions of one and the same Kuramoto system (1.2) under one and the same phase normalization (1.11). The theoretical justification for this operation are the shadowing properties which come with Morse–Smale

transversality. See for example the techniques summarized in [GPS02, PPT12], and the many earlier references there.

In figure 2.5 we have illustrated theorem 2.9 on swarming rebellions from a 2-cluster equilibrium  $\Theta_-$  at  $t \rightarrow -\infty$  towards a 2-cluster equilibrium  $\Theta_+$  with larger fat cluster size. We have partitioned  $N = 21$  oscillators  $\vartheta_*(t) : \Theta_- \rightsquigarrow \Theta_+$  into  $M = 11$  clusters of sizes  $N_1 = N_- = 11$ ,  $N_2 = \dots = N_M = 1$ , and  $N_+ = 20$ . Specifically, the cluster decomposition (1.8) reads  $J_- = J_1 := \{1, \dots, 11\}$ , and  $J_m := \{10 + m\}$  for  $2 \leq m \leq 11$ . Note  $J_M = J_+^c = \{21\}$  and  $\hat{J} = J_2 \cup \dots \cup J_{M-1} = \{12, \dots, 20\}$ . Consider partitioned coordinates

$$(7.6) \quad (\hat{x}, x_M, \xi_1, \hat{\xi})$$

with respect to the index partition  $J_1 \dot{\cup} \hat{J} \dot{\cup} J_M$ ; compare (3.5). We omit  $\xi_M = 0$ , because the one-man cluster  $J_M = \{21\}$  is represented by its “average”  $x_M$ . As usual, we have omitted the average  $x_1$  over  $J_1$ , by normalization (1.11). In coordinates (7.6):

$$(7.7) \quad \begin{aligned} \vartheta_*(t) &\in \text{Fix}(S_{J_-}) \cap \text{Fix}(S_{J_+^c}) = \{\xi_1 = 0\}; \\ \Theta_- &= (11/21, 11/21, 0, 0)\pi; \\ \Theta_+ &= (-1/21, 20/21, 0, 0)\pi. \end{aligned}$$

As usual, we pick the initial perturbation

$$(7.8) \quad \vartheta_*(0) = \Theta_+ + \varepsilon(\hat{x}, 0, 0, \hat{\xi}) \in \text{Fix}(S_{J_-}) \cap \text{Fix}(S_{J_+^c}),$$

as an approximation of the stable manifold  $W_+^s$  of  $\Theta_+$ ; see lemma 4.2(i), (4.2), and (4.8). We then solve (1.2) backwards in time, where (4.1) and (4.4) ensure  $\vartheta_*(0) \in W_-^u$  and hence convergence of  $\vartheta_*(t)$  to  $\Theta_-$ , for  $t \rightarrow -\infty$ . Here we use existence of the heteroclinic orbit constructed in theorem 2.9, to guarantee that the closure of the unstable manifold  $W_-^u$  of  $\Theta_-$  extends to  $\Theta_+$ , at all. In case the whole rebellion is required to swarm out towards the same side of  $x_M$ , unilaterally left or right, we choose a perturbation with nonzero average component  $\hat{x}$ , of the appropriate sign, and then a perturbation  $|\hat{\xi}| \ll |\hat{x}|$  of zero average to exclude clustering within the swarm. To realize general prescribed sign configuration (6.5) of  $\hat{\xi}$ , we let  $\hat{x} = 0$ . To avoid relabeling of oscillators  $2, \dots, M-1$ , we then choose the first  $m_* - 1$  nonzero components of the perturbation  $\hat{\xi}$  on  $\hat{J}$  negative, and the remaining  $M - 1 - m_*$  nonzero components positive. The zero average condition on  $\hat{\xi}$  is easily respected here.

Simulation code has been implemented in *Julia* [BEKS17]. All figures are generated using the package *Plots.jl*. We integrate by using the explicit 4th-order Runge–Kutta method in the package *DifferentialEquations.jl* with fixed step size  $10^{-2}$ . We have made the code more human readable using *Cursor* as an AI aid to arrange documentations.

## 8 Discussion

### 8.1 Transients and perturbations

We have considered the classical Kuramoto model (1.1) with equal frequencies  $\omega_j = \omega$  and order parameter  $R \geq R_0 > 0$ :

$$(8.1) \quad \dot{\vartheta}_j = \omega + \frac{1}{N} \sum_{k=1}^N \sin(\vartheta_k - \vartheta_j),$$

for  $j = 1, \dots, N$ . Our results address an uncharted, yet fundamental, problem regarding global dynamics. Specifically, we have explored the complicated transients from a plethora of partially synchronized equilibria to total synchrony. The consequences of our approach and results are at least three-fold.

*First*, the transients to total synchrony involve concatenations of successive rebellions among unstable, or “metastable” 2-cluster configurations. This is not accessible to the Watanabe–Strogatz transformation, which excludes any heteroclinic orbits between 2-cluster equilibria. Our alternative approach is complementary, and is based on the presence of a dominating, fat cluster.

*Second*, for  $R > 0$ , corollary 2.5 has established structural stability of the original Morse–Smale system (8.1) in the full angle space  $\mathbb{T}^N$ . This yields  $C^0$  orbit equivalent flows under *all*  $C^1$ -small perturbations of the Kuramoto model (8.1). In particular, we may consider small deviations (1.1) from the single frequency regime  $\omega_j \equiv \omega$ . Any permutation-equivariance from  $S_N$  is then lost, and the total synchrony of the single-frequency model (also called *phase synchronization*) fails. The weaker notion of *frequency synchronization*,

$$(8.2) \quad \lim_{t \rightarrow \infty} \sup_{i,j=1,\dots,N} |\dot{\vartheta}_i(t) - \dot{\vartheta}_j(t)| = 0,$$

however, persist, for any solutions with  $R > 0$ . This follows from in-phase convergence towards periodic orbits, because all periodic orbits remain rigidly rotating waves under small perturbations. Indeed, this is caused by the remaining  $\mathbb{S}^1$ -equivariance (1.3), even when equivariance under any permutations in  $S_N$  has been destroyed, completely.

Much more general than the original model (8.1), consider perturbations of the form

$$(8.3) \quad m_j \ddot{\vartheta}_j + \dot{\vartheta}_j = \omega_j + \frac{K}{N} \sum_{k=1}^N \sin(\vartheta_k(t - \tau_{jk}) - \vartheta_j(t - \tilde{\tau}_{jk}) - \gamma_{jk});$$

see [DöBu12, HKL14, HKP15, HsJuKw19, HJKU20]. Assume that frequency deviations  $|\omega_j - \omega|$ , inertiae  $m_j \geq 0$ , time delays  $\tau_{jk}, \tilde{\tau}_{jk} \geq 0$ , and phase lags  $|\gamma_{jk}|$  are all small. The resulting slow inertial manifold, in the sense of Fenichel theory [Jo95], is then invariant and exponentially attracting. The resulting slow global dynamics, on it, therefore amounts to a  $C^1$ -small perturbation of the structurally stable single-frequency model (8.1), again for order parameters  $R > 0$ . Notably, positive time delays infinitely increase the dimensionality of the phase space. Nevertheless, the above approach admits small delays as well; see [Chic03]. Early results on the elimination of small delays in nonlinear equations go back

as far as [Kur67]. Morse–Smale structural stability then admits small perturbations of the general form (8.3), by corollary 2.5.

*Third*, our approach is based on all-to-all  $S_N$ -equivariance and the existence of Lyapunov functions. Transversality follows from the somewhat surprising observation that invariant manifolds of cluster equilibria are contained, globally, in linear subspaces characterized by invariance under certain subgroups of  $S_N$ , and share the same dimension with such linear fix-spaces. Many other variants of the Kuramoto model also retain at least some permutation-equivariance, and a Lyapunov function. Examples are more general network topologies defined by weighted coupling constants  $K_{ij} \geq 0$  (see [ChHsHs24]), or by inertial terms. We have not yet ventured into these vast areas, systematically.

## 8.2 Comparison with Stuart–Landau oscillators

We conclude with a comparison to previous results on *local*  $S_N$  symmetry-breaking among  $N$  nonlinear complex Stuart–Landau oscillators with linear all-to-all coupling. These results have been derived and proved for the dynamics of 3-clusters, in the limit of large  $N$ . For complete details, see [KFHK20, FHK21] and the references there.

The Stuart–Landau system reads

$$(8.4) \quad \dot{W}_j = (1 - (1 + i\gamma)|W_j|^2)W_j + \beta \frac{1}{N} \sum_{k=1}^N (W_k - W_j).$$

Here  $W_j \in \mathbb{C}$  indicate phase and amplitude of the  $j$ -th oscillator,  $j = 1, \dots, N$ . We consider real amplitude dependence  $\gamma \neq 0$  of individual periods, and complex coupling  $\beta \in \mathbb{C}$ . Note equivariance of (8.4) under the action of  $\sigma \in S_N$ , analogously to (1.5).

For a background and motivation, we recall how (8.4) often serves, in physics, as a “normal form” for oscillatory systems close to the onset of oscillation and under the influence of a linear coupling through the mean field [Kur84, GMK08]. This normal form has been established to be a good approximation in a multitude of contexts from various disciplines, whether it be in physics, chemistry, biology, neuroscience, social dynamics, or engineering. For an overview see e.g. [PRK03, PiRo15] or references 1–15 in [KGO15].

We address bifurcation from the totally synchronous 1-cluster solution  $W_j(t) := \exp(-i\gamma t)$ . The Benjamin–Feir instability describes destabilization due to the appearance of a Floquet exponent zero of high (nontrivial) multiplicity  $N - 1$ . Explicit center manifold reduction, in suitable coordinates, and truncation to polynomial order 3, lead to a reduced real system of the general form

$$(8.5) \quad \dot{y}_j = f_j(\mathbf{y}) := (\lambda + c \cdot \langle y^2 \rangle) y_j + \tilde{y}_j^2 + \tilde{y}_j^3$$

for  $\mathbf{y} \in \mathbf{Y} := \mathbb{R}^N$ . We use the abbreviations  $\langle y^p \rangle$  and  $\tilde{x}_j^p := x_j^p - \langle x^p \rangle$  for the averages of  $p$ -th powers and the deviations from their average, respectively. The real parameter  $\lambda$  is the linearization at the trivial equilibrium  $\mathbf{y} = 0$  of total synchrony, which corresponds to the reference 1-cluster synchronous periodic orbit  $W$ . The Benjamin–Feir instability of  $\mathbf{y} = 0$  occurs at  $\lambda = 0$ . Notice that the zero sum space  $\mathbf{Y}_0 := \{\langle y \rangle = 0\}$  is indeed invariant, not only under the linear action (1.5) of the group  $S_N$ , but also under the nonlinear dynamics



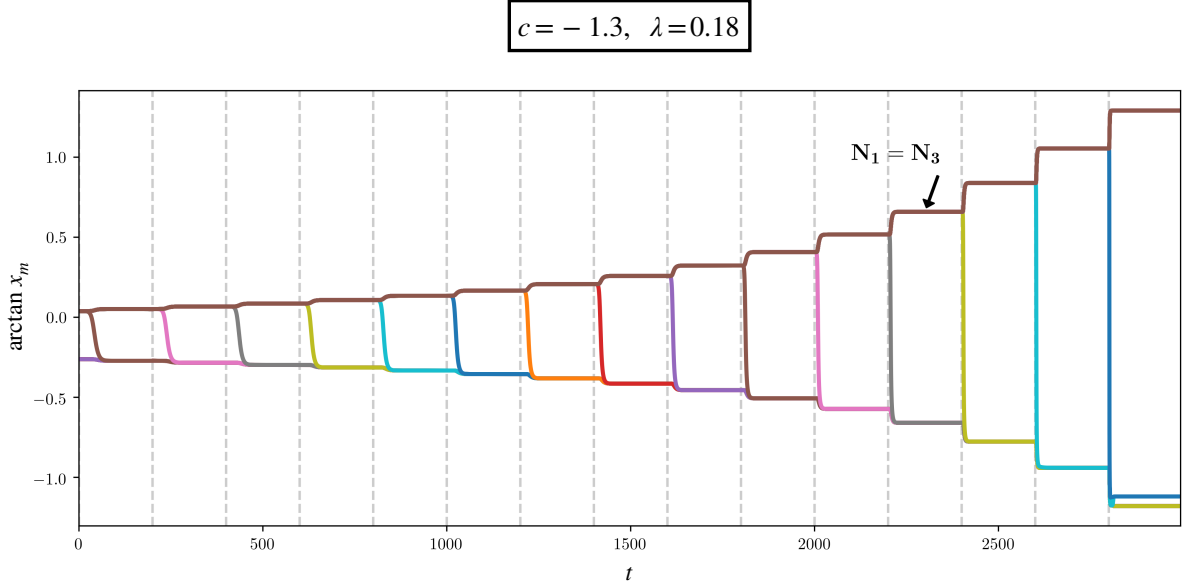


**Figure 8.1:** *Heteroclinic rebel transients obtained from numerical simulations of (8.5) for  $c = -1.3$ ,  $\lambda = 0.18$  and  $N = 32$  oscillators. See section 5 of [FKHK21] for details. The graphs indicate 3-cluster solutions (8.7) with one-man rebel cluster  $x_2 = y_n$ ,  $n = N_1 + 1$ . Starting from  $N_1 = 4$ , we apply a small random perturbation to  $y_n = \xi_3$  at a time indicated by the dashed vertical lines, only. We then integrate the system (8.5) with rebel  $y_n \neq \xi_1, \xi_3$ , until the dynamics settles again. See the colored rebel transients of  $x_2 = y_n$  from  $x_3$  (top) to  $x_1$  (bottom), along which the rebel  $x_2 = y_n$  changes its cluster affiliation. Updating  $N_1 \mapsto N_1 + 1$  and  $n \mapsto n + 1$ , we repeat this process until instability to a 3-cluster equilibrium takes over from  $N_1 = 18$ .*

of (8.5). Indeed  $\langle y \rangle = \langle \tilde{y}_j^p \rangle = 0$  on  $\mathbf{Y}_0$ . See [Elm01, DiSt03, StElCo03, Elm04, GoSt23] for analysis of equilibrium bifurcations.

The importance of (8.5) reaches far beyond the Stuart–Landau context, or any direct interpretation as a network of  $N$  identical scalar “cells” with all-to-all coupling via power sums. For example, [Elm01, StElCo03] encounter (8.5) in the context of biological evolution of sympatric speciation. In fact, steady-state bifurcation analysis of any fully permutation-symmetric network, at eigenvalue 0, typically leads to irreducible eigenspaces. Beyond total synchrony  $y_1 = \dots = y_N$ , the standard representation on  $\mathbf{Y}_0$  provides the simplest interesting case. Up to scaling and possible time-reversal, in fact, (8.5) on  $\mathbf{Y}_0$  represents the most general cubic vector field which is equivariant under the standard representation (1.5) of  $S_N$  on  $\mathbf{Y}_0$ . Just based on linearization at total synchrony, rather than the computational intricacies of center manifold reduction, it is therefore not surprising that all-to-all Stuart–Landau coupling (8.4) leads to (8.5). The explicit computations in [FKHK21] show the Stuart–Landau setting (8.4) to be universal, in the sense that all real higher order coefficients  $c$ , and all bifurcation parameters  $\lambda$  near  $\lambda = 0$  actually arise, for suitable parameters  $\gamma \in \mathbb{R}$  and  $\beta \in \mathbb{C}$ .

The cubic truncation (8.5) possesses an explicit *gradient structure*. In fact, *all*  $S_N$ -equivariant polynomial vector fields  $\mathbf{f}$  on the standard representation  $\mathbf{Y}_0$ , up to and including order three, are gradients of scalar invariants. For higher orders, in contrast, that gradient property fails.



The gradient property allowed [KFHK20, FKHK21] to study the dynamics of (8.5), in terms of clustering and rebellions among cluster equilibria, much in the spirit of our present approach to the Kuramoto model (1.2). Globally, [KFHK20] classifies the cluster dynamics of (8.5) by seven different nondegenerate cases, depending on the location of

$$(8.6) \quad c \in \mathbb{R} \setminus \{-2, -3/2, -4/3, -5/4, -1, -1/2\}.$$

For  $N = 32$  oscillators, figure 8.1 illustrates the choice  $-4/3 < c = -1.3 < -5/4$  at  $\lambda = 0.18$ . In the spirit of figures 2.2–2.3, the 3-cluster dynamics of successive one-man rebellions is documented by their heteroclinic transients between two large clusters near equilibrium. We use the cluster notation (1.9)–(1.11), analogously, to denote the three clusters

$$(8.7) \quad \begin{aligned} x_1 &:= y_1 = \cdots = y_{N_1}, \\ x_2 &:= y_n, \\ x_3 &:= y_{n+1} = \cdots = y_N = x_3, \end{aligned}$$

with the abbreviation  $n = N_1 + 1$ . We start from  $x_2 = x_3$ . For  $N_1 = 4$ , initially, this corresponds to a *small* initial size fraction  $\alpha_1 = N_1/N = 0.125$ . After a small random perturbation of the single component  $y_n$  in cluster  $x_2$ , we integrate the clustered ODE (8.5) forward in time until the dynamics appears to settle. As a result, we observe heteroclinic rebel dynamics, that is, the perturbed oscillator  $y_n$  changes its cluster affiliation from the large cluster at  $x_3$  to the small cluster at  $x_1$ . In other words,  $N_1 = 5$ , after the rebel transient. Note that the heteroclinic defection transition, from majority cluster to minority cluster occurs in the opposite direction of the Kuramoto model (1.2); compare section 2. Updating  $N_1 \mapsto N_1 + 1$  and  $n \mapsto n + 1$ , we repeat this process for increasing cluster sizes  $N_1$ . Note the successive heteroclinic transients of the rebels  $y_n$ , from  $x_3$  down to  $x_1 < x_3$ .

After 12 rebellions, of course, equal cluster parity  $N_1 = N_2 = 16$  is reached and the former minority cluster  $x_1$  reaches and overtakes majority. After 14 transients, the dynamics enters a bifurcation region towards 3-cluster equilibria. At that stage, the third coexisting cluster of (8.5), at  $x_2 < x_3$  near  $x_1 < x_2$ , consists of just one single rebel. Such 3-cluster equilibria cannot occur in the Kuramoto model (1.2). The resulting dynamics in the Stuart–Landau case (8.4) have not been analyzed, as yet.

## References

- [ABP05] J.A. Acebrón, L.L. Bonilla, C.J. Pérez Vicente, F. Ritort, and R. Spigler. The Kuramoto model: A simple paradigm for synchronization phenomena. *Rev. Mod. Phys.* **77** (2005), 137–185; <https://doi.org/10.1103/RevModPhys.77.137>
- [ADLY25] Ch. Adwani, R. De Leo, and J.A. Yorke. What is the graph of a dynamical system? *Nonlin. Dyn.* (2025); <https://doi.org/10.1007/s11071-025-11466-9>
- [Arn88] V.I. Arnold. *Geometrical Methods in the Theory of Ordinary Differential Equations*. Springer-Verlag, Berlin 1988.
- [AOWT07] P. Ashwin, G. Orosz, J. Wordsworth, and S. Townley. Dynamics on Networks of Cluster States for Globally Coupled Phase Oscillators. *SIAM J. Appl. Dyn. Syst.* **6** (2007), 728–758; <https://doi.org/10.1137/070683969>

- [Beyn90] W.-J Beyn. The numerical computation of connecting orbits in dynamical systems. *IMA J. Numer. Analysis* **10** (1990), 379–405.
- [BEKS17] J. Bezanson, A. Edelman, S. Karpinski, and V. B. Shah. Julia: a fresh approach to numerical computing. *SIAM Review* **59** (2017), 65–98.
- [BroStr18] D. Brockmann and S. Strogatz. *Ride my Kuramoto cycle*. Web app (2018). <https://www.complexity-explorables.org/explorables/ride-my-kuramoto-cycle/>
- [BrFie88] P. Brunovský and B. Fiedler. Connecting orbits in scalar reaction diffusion equations. *Dynamics Reported* **1** (1988), 57–89.
- [BrFie89] P. Brunovský and B. Fiedler. Connecting orbits in scalar reaction diffusion equations II: The complete solution. *J. Diff. Eqns.* **81** (1989), 106–135.
- [ChHsHs24] S.-H. Chen, C.-H. Hsia, and T.-Y. Hsiao. Complete and partial synchronization of two-group and three-group Kuramoto oscillators. *SIAM J. Appl. Dyn. Syst.* **23** (2024), no. 3, 1586–1613; <https://doi.org/10.1137/23M1586227>
- [Chib15] H. Chiba. A proof of the Kuramoto conjecture for a bifurcation structure of the infinite-dimensional Kuramoto model. *Ergod. Th. Dynam. Sys.* **35** (2015), 762–834; <https://doi.org/10.1017/etds.2013.68>
- [Chic03] C. Chicone. Inertial and slow manifolds for delay equations with small delays. *J. Differ. Equ.* **190** (2003), 364–406; [https://doi.org/10.1016/S0022-0396\(02\)00148-1](https://doi.org/10.1016/S0022-0396(02)00148-1)
- [ChoLau00] P. Chossat and R. Lauterbach. *Methods in Equivariant Bifurcations and Dynamical Systems*. World Scientific, Singapore 2000.
- [ChoHa82] S.-N. Chow and J.K. Hale. *Methods of Bifurcation Theory*. Springer-Verlag, New York 1982.
- [Con78] C.C. Conley. *Isolated Invariant Sets and the Morse Index*. AMS, Providence R.I. 1978.
- [DLY24] R. De Leo and J.A. Yorke. Streams and graphs of dynamical systems. *Qual. Theory Dyn. Syst.* **24** (2024); <https://doi.org/10.1007/s12346-024-01112-x>
- [DGGK03] A. Dhooge, W. Govaerts, and Yu.A. Kuznetsov. MATCONT: A MATLAB package for numerical bifurcation analysis of ODEs. *ACM Trans. Math. Softw.* **29** (2003), 141–164.
- [DiSt03] A.P.S. Dias and I. Stewart. Secondary bifurcations in systems with all-to-all coupling. *Proc. R. Soc. Lond. A* **459** (2003), 1969–1986, <https://doi.org/10.1098/rspa.2002.1103>
- [DoXu13] J.-G. Dong and X. Xue. Synchronization analysis of Kuramoto oscillators. *Commun. Math. Sci.* **11** (2013), no. 2, 465–480; <https://dx.doi.org/10.4310/CMS.2013.v11.n2.a7>
- [DöBu12] F. Dörfler and F. Bullo. Synchronization and transient stability in power networks and nonuniform Kuramoto oscillators. *SIAM J. Control Optim.* **50** (2012), no. 3, 1616–1642; <https://doi.org/10.1109/ACC.2010.5530690>
- [Elm01] T. Elmhirst. *Symmetry and Emergence in Polymorphism and Sympatric Speciation*. PhD Thesis, Warwick 2001.
- [Elm04] T. Elmhirst.  $S_N$ -equivariant symmetry-breaking bifurcations. *Int. J. Bifurcation Chaos* **14** (2004), 1017–1036.
- [Fie88] B. Fiedler. *Global Bifurcation of Periodic Solutions with Symmetry*. Lect. Notes Math. **1309**, Springer-Verlag, Heidelberg 1988.
- [Fie94] B. Fiedler. Global attractors of one-dimensional parabolic equations: sixteen examples. *Tatra Mountains Math. Publ.* **4** (1994), 67–92.
- [Fie02] B. Fiedler (ed.). *Handbook of Dynamical Systems* **2**. Elsevier, Amsterdam 2002.
- [FKHK21] B. Fiedler, F.P. Kemeth, S.W. Haugland, K. Krischer. Global heteroclinic rebel dynamics among large 2-clusters in permutation equivariant systems. *SIAM Appl. Dyn. Systems* **20** (2021), 1277–1319; <https://doi.org/10.1137/20M1361493>
- [FieRo96] B. Fiedler and C. Rocha. Heteroclinic orbits of semilinear parabolic equations. *J. Differ. Eqs.* **125** (1996), 239–281.
- [FieRo20] B. Fiedler and C. Rocha. Boundary orders and geometry of the signed Thom–Smale complex

- for Sturm global attractors. *J. Dyn. Differ. Eqs.* (2020), 2787–2818; <https://doi.org/10.1007/s10884-020-09836-5>
- [FieRo23] B. Fiedler and C. Rocha. Design of Sturm global attractors 1: Meanders with three noses, and reversibility. *Chaos* **33**, 083127 (2023); <https://doi.org/10.1063/5.0147634>
- [FieRo24] B. Fiedler and C. Rocha. Design of Sturm global attractors 2: Time-reversible Chafee-Infante lattices of 3-nose meanders. *São Paulo J. Math. Sciences.* (2024), 975–1014; <https://doi.org/10.1007/s40863-023-00385-5>
- [FrM88] R.D. Franzosa and K. Mischaikow. The connection matrix theory for semiflows on (not necessarily locally compact) metric spaces. *J. Diff. Eqs.* **71** (1988), 270–287.
- [GMK08] V. García-Morales and K. Krischer. Normal-form approach to spatiotemporal pattern formation in globally coupled electrochemical systems. *Phys. Rev.* **E 78** (2008), 057201.
- [GoStSch88] M. Golubitsky, I. Stewart, and D.G. Schaeffer. *Singularities and groups in bifurcation theory. II*. Springer-Verlag, New York 1988.
- [GoSt02] M. Golubitsky and I. Stewart. *The Symmetry Perspective*. Birkhäuser, Basel 2002.
- [GoSt23] M. Golubitsky and I. Stewart. *Dynamics and Bifurcation in Networks. Theory and Applications of Coupled Differential Equations*. SIAM, Philadelphia 2023.
- [GPS02] C. Grebogi, L. Poon, T. Sauer et al. Shadowability of chaotic dynamical systems. In [Fie02], 313–344.
- [HKP15] S.-Y. Ha, H. Kim, and J. Park. Remarks on the complete frequency synchronization of Kuramoto oscillators. *Nonlinearity* **28** (2015), 1441–1462; <https://doi.org/10.1088/0951-7715/28/5/1441>
- [HKL14] S.-Y. Ha, Y. Kim, and Z. Li. Large-time dynamics of Kuramoto oscillators under the effects of inertia and frustration. *SIAM J. Appl. Dyn. Syst.* **13** (2014), no. 1, 466–492; <https://doi.org/10.1137/130926559>
- [HMO02] J.K. Hale, L.T. Magalhães, and W.M. Oliva. *Dynamics in Infinite Dimensions*. 2nd ed. Springer-Verlag, New York 2002.
- [vHeWre93] J.L. van Hemmen and W.F. Wreszinski. Lyapunov function for the Kuramoto model of nonlinearly coupled oscillators. *J. Stat. Phys.* **27** (1993), 145–166.
- [HsJuKw19] C.-H. Hsia, C.-Y. Jung, and B. Kwon. On the synchronization theory of Kuramoto oscillators under the effect of inertia. *J. Differ. Equ.* **267** (2019), 742–775; <https://doi.org/10.1016/j.jde.2019.01.024>
- [HJKU20] C.-H. Hsia, C.-Y. Jung, B. Kwon, and Y. Ueda. Synchronization of Kuramoto oscillators with time-delayed interactions and phase lag effect. *J. Differ. Equ.* **268** (2020), 7897–7939; <https://doi.org/10.1016/j.jde.2019.11.090>
- [Jo95] C. Jones. *Geometric singular perturbation theory*. In R. Johnson (Ed.), *Dynamical Systems*, Lecture Notes in Mathematics, **1609**, 44–118. Springer, Berlin 1995.
- [KaMM04] T. Kaczynski, K. Mischaikow, and M. Mrozek. *Computational Homology*. Springer-Verlag, New York 2004.
- [KFHK20] F.P. Kemeth, B. Fiedler, S.W. Haugland, and K. Krischer. 2-cluster fixed-point analysis of mean-coupled Stuart–Landau oscillators in the center manifold of the Benjamin–Feir instability. *J. Phys. Complex.* (2020); <https://doi.org/10.1088/2632-072X/abd0da>
- [KOD05] B. Krauskopf, H.M. Osinga, E.J. Doedel, et al. A survey of methods for computing (un)stable manifolds of vector fields. *Int. J. Bif. Chaos Appl. Sci. Eng.* **15** (2005), 763–791.
- [KGO15] W. Lim Ku, M. Girvan, and E. Ott. Dynamical transitions in large systems of mean field-coupled Landau-Stuart oscillators: Extensive chaos and cluster states. *Chaos* **25** 123122 (2015); <https://doi.org/10.1063/1.4938534>
- [Kur75] Y. Kuramoto. Self-entrainment of a population of coupled non-linear oscillators. *Int. Symp. Math. Probl. Theor. Phys.*, H. Arakai (ed), Kyoto 1975, 420–422.
- [Kur84] Y. Kuramoto. *Chemical Oscillations, Waves, and Turbulence*. Springer-Verlag, Berlin, 1984.

- [KurB02] Y. Kuramoto and D. Battogtokh. Coexistence of coherence and incoherence in nonlocally coupled phase oscillators. *Nonlin. Phenom. Complex Syst.* **5** (2002), 380–385.
- [Kurz67] J. Kurzweil. Invariant manifolds for flows. *Differ. Equations Their Appl.* (1967), Bratislava: Slovenské pedagogické nakladateľstvo, 89–92.
- [Lin90] X.-B. Lin. Using Melnikov’s method to solve Silnikov’s problems. *Proc. R. Soc. Edinb. A: Math.* **116** (1990), 295–325; <https://doi.org/10.1017/S0308210500031528>
- [Lin08] X.-B. Lin. Lin’s method. *Scholarpedia* (2008); [http://www.scholarpedia.org/article/Lin%27s\\_method](http://www.scholarpedia.org/article/Lin%27s_method)
- [McCSoh11] J.M. McCarthy and G.S. Soh. *Geometric Design of Linkages*. Springer-Verlag, New York 2011.
- [MM02] K. Mischaikow and M. Mrozek. Conley index. In [Fie02], 393–460.
- [Pa69] J. Palis. On Morse–Smale dynamical systems. *Topology* **8** (1969), 385–404.
- [PdM82] J. Palis and W. de Melo. *Geometric Theory of Dynamical Systems. An Introduction*. Springer-Verlag, New York 1983.
- [PaSm70] J. Palis and S. Smale. Structural stability theorems. In *Global Analysis*, S. Chern, S. Smale (eds.). Proc. Symp. in Pure Math. vol. XIV. AMS, Providence 1970.
- [PPT12] K.J. Palmer, S.Yu. Pilyugin, and S.B. Tikhomirov. Lipschitz shadowing and structural stability of flows. *J. Diff. Eqs.* **252** (2012), 1723–1747.
- [PiRo09] A. Pikovsky and M. Rosenblum. Self-organized partially synchronous dynamics in populations of nonlinearly coupled oscillators. *Physica D* **238** (2009), 27–37; <https://doi.org/10.1016/j.physd.2008.08.018>
- [PiRo15] A. Pikovsky and M. Rosenblum. Dynamics of globally coupled oscillators: Progress and perspectives. *Chaos* **25** (2015), 097616; <https://doi.org/10.1063/1.4922971>
- [PRK03] A. Pikovsky, M. Rosenblum, and J. Kurths. *Synchronization: A Universal Concept in Non-linear Sciences*. Cambridge University Press, 2003.
- [Rau02] G. Raugel. Global attractors in partial differential equations. In [Fie02], 885–982.
- [RFLN25] C. Rocha, B. Fiedler, and A. López-Nieto. A classification of global attractors for  $\mathbb{S}^1$ -equivariant parabolic equations. (2025); <https://arxiv.org/abs/2507.10051>
- [StElCo03] I. Stewart, T. Elmhirst, J. Cohen. Symmetry-breaking as an origin of species. In *Bifurcation, Symmetry and Patterns*, J. Buescu et al (eds.). Birkhäuser, Basel 2003, 3–54.
- [Str03] S.H. Strogatz. *Sync: The Emerging Science of Spontaneous Order*. Hyperion, New York 2003.
- [Van82] A. Vanderbauwhede. *Local Bifurcation and Symmetry*. Pitman, Boston 1982.